Elsevier Editorial System(tm) for Biomaterials

Manuscript Draft

Manuscript Number: jbmt32929R1

Title: Enabling Dual Cellular Destinations of Polymeric Nanoparticles for Treatment Following Partial Injury to the Central Nervous System

Article Type: FLA Original Research

Section/Category: Biomaterials for the Delivery of Drugs, Genes, Vaccines and Active Biomolecules (BDGV)

Keywords: Polymer nanoparticles; Central nervous system injury; oxidative stress and aquaporin4; targeted drug delivery of antioxidants; Nanoscale secondary ion mass spectroscopy; macrophages

Corresponding Author: Dr. Melinda Fitzgerald, PhD

Corresponding Author's Institution: The University of Western Australia

First Author: Ivan Lozic

Order of Authors: Ivan Lozic; Richard Hartz; Carole Bartlett; Jeremy Shaw; Michael Archer; Priya Naidu; Nicole Smith; Sarah Dunlop; Swaminathan Iyer; Matt Kilburn; Melinda Fitzgerald, PhD

Abstract: Following neurotrauma, oxidative stress is spread via the astrocytic syncytium and is associated with increased aquaporin 4 (AQP4), inflammatory cell infiltration, loss of neurons and glia and functional deficits. Herein we evaluate multimodal polymeric nanoparticles functionalized with an antibody to an extracellular epitope of AQP4, for targeted delivery of an anti-oxidant as a therapeutic strategy following partial optic nerve transection. Using fluorescence microscopy, spectrophotometry, correlative nanoscale secondary ion mass spectrometry (NanoSIMS) and transmission electron microscopy, in vitro and in vivo, we demonstrate that functionalized nanoparticles are coated with serum proteins such as albumin and enter both macrophages and astrocytes when administered to the site of a partial optic nerve transection in rat. Antibody functionalized nanoparticles synthesized to deliver the antioxidant resveratrol are effective in reducing oxidative damage to DNA, AQP4 immunoreactivity and preserving visual function. Non-functionalized nanoparticles evade macrophages more effectively and are found more diffusely, including in astrocytes, however they do not preserve the optic nerve from oxidative damage or functional loss following injury. Our study highlights the need to comprehensively investigate nanoparticle location, interactions and effects, both in vitro and in vivo, in order to fully understand functional outcomes.

MANDATORY AUTHOR DECLARATION

An Author Declaration is a mandatory part of a submission. This Declaration covers a number of logistic and ethical issues which are described below. A template for the covering letter will be found at the end of this document. Authors may save this template, obtain the required signatures and then upload it as a part of their submission.

Corresponding Author
The name, address, and valid email address of the corresponding author. The Corresponding Author is the person who is responsible for the manuscript as it moves through the journal's submission process. This person must be registered with Editorial Manager as all correspondence pertaining to the manuscript will be sent to him/her via the system. *The Corresponding Author is the person responsible for making any edits/submitting revisions to the manuscript and is the only author who may view the progress of the manuscript as it moves from one stage to the next. He/she is responsible for communicating with the other authors about progress, revisions and final approval of the proofs and is the only authorised contact with the Editorial Office.*

Redundant or Duplicate Publication
Redundant or duplicate publication is publication of a paper that overlaps substantially with one already published. If redundant or duplicate publication is attempted or occurs without notification to the Editor, authors should expect editorial action to be taken.

When submitting a paper, the author should always make a full statement to the editor about all submissions and previous papers that might be regarded as redundant or duplicate publication of the same or very similar work. The author should alert the editor if the work includes subjects about which a previous paper has been published. Any such work should be referred to and referenced in the new paper. Copies of such material, including papers in press, should be included with the submitted paper to assist the editor in determining how to handle the matter.

Authorship
It is required that the Author Declaration be signed by all authors. All persons designated as authors should qualify for authorship, and all those who qualify should be listed. Each author should have participated sufficiently in the work to take public responsibility for appropriate portions of the content. The corresponding author should take responsibility for the integrity of the work as a whole, from inception to published article.
Authorship credit should be based only on 1) substantial contributions to conception and design, or acquisition of data, or analysis and interpretation of data; 2) drafting the article or revising it critically for important intellectual content; and 3) final approval of the version to be published. Conditions 1, 2, and 3 must all be met.

The order of authorship on the by-line is a matter for the institution(s) and must be agreed by all named authors prior to submission.

Addition, deletion, or rearrangement of author names in an accepted manuscript's authorship

Note that The Lancet, Cell, and journals published by Elsevier on behalf of learned societies may have different policies.

<u>Before the accepted manuscript is published in an online issue</u>

Requests to add or remove an author, or to rearrange the author names, must be sent to the Journal Manager from the corresponding author of the accepted manuscript and must include:

(a) The reason the name should be added or removed, or the author names rearranged.

MANDATORY AUTHOR DECLARATION

(b) Written confirmation (email, fax, letter) from all authors that they agree with the addition, removal or rearrangement. In the case of addition or removal of authors, this includes confirmation from the author being added or removed.

Requests that are not sent by the corresponding author will be forwarded on by the Journal Manager to the corresponding author, who must follow the procedure as described above.

Note that:

- Journal managers will inform Editors of any such requests
- Publication of the accepted manuscript in an online issue is suspended until authorship has been agreed

After the accepted manuscript is published in an online issue

Any requests to add, delete, or rearrange author names in an article published in an online issue will follow the same policies as noted above and result in a corrigendum.

Conflict of Interest

Author conflict of interest for a given manuscript exists when an author has ties to activities that could inappropriately influence his or her judgment, whether or not judgment is in fact affected. Financial relationships with industry are usually considered to be the most important conflicts of interest.

When submitting a manuscript authors are responsible for recognizing and disclosing financial and other conflicts of interest that might bias their work. They should acknowledge in the manuscript all financial support for the work and other financial or personal connections to the work. If there are no such conflicts or financial support to acknowledge, the authors should declare this by the following statement: *The authors confirm that there are no known conflicts of interest associated with this publication and there has been no significant financial support for this work that could have influenced its outcome.*

Ethical Issues

When reporting experiments on animals, authors should indicate whether the institution's or a national research council's guide for, or any national law on, the care and use of laboratory animals was followed. When reporting experiments on human subjects, authors should indicate whether the procedures followed were in accordance with the ethical standards of the responsible committee on human experimentation (institutional or regional) and with the Helsinki Declaration of 1975, as revised in 1983.

This means that the authors must make a clear statement that the laws which apply to them in their own country were followed. This is best done as a statement under the section Materials & Methods.

Acknowledgements

All contributors who do not meet the criteria for authorship, such as a person who provided purely technical help, writing assistance, or a department chair who provided only general support should be listed in the acknowledgments. Financial and material support should also be recognised in the acknowledgments.

Impact Statement

Authors are encouraged to include in their covering letter a statement of their understanding of the importance and impact of their work. This should not be speculation on vague possibilities for clinical use but a precise statement relating to the underlying science. A concise statement of this impact should be included at the end of the Abstract.

AUTHOR DECLARATION TEMPLATE

We the undersigned declare that this manuscript is original, has not been published before and is not currently being considered for publication elsewhere.

We wish to confirm that there are no known conflicts of interest associated with this publication and there has been no significant financial support for this work that could have influenced its outcome.

We confirm that the manuscript has been read and approved by all named authors and that there are no other persons who satisfied the criteria for authorship but are not listed. We further confirm that the order of authors listed in the manuscript has been approved by all of us.

We confirm that we have given due consideration to the protection of intellectual property associated with this work and that there are no impediments to publication, including the timing of publication, with respect to intellectual property. In so doing we confirm that we have followed the regulations of our institutions concerning intellectual property.

We further confirm that any aspect of the work covered in this manuscript that has involved either experimental animals or human patients has been conducted with the ethical approval of all relevant bodies and that such approvals are acknowledged within the manuscript.

We understand that the Corresponding Author is the sole contact for the Editorial process (including Editorial Manager and direct communications with the office). He/she is responsible for communicating with the other authors about progress, submissions of revisions and final approval of proofs. We confirm that we have provided a current, correct email address which is accessible by the Corresponding Author and which has been configured to accept email from biomaterials@elsevier.com.

Signed by all authors as follows:

		Date
Ivan Lozić,		7/5/2015
Richard V. Hartz,		
Carole A. Bartlett,		7/5/2015
Jeremy A. Shaw,		
Michael Archer,		7/5/2015
Priya S.R. Naidu,		8/5/2015
Nicole M. Smith,		06/05/2015
Sarah A. Dunlop,	See over	

AUTHOR DECLARATION TEMPLATE

We the undersigned declare that this manuscript is original, has not been published before and is not currently being considered for publication elsewhere.

We wish to confirm that there are no known conflicts of interest associated with this publication and there has been no significant financial support for this work that could have influenced its outcome.

We confirm that the manuscript has been read and approved by all named authors and that there are no other persons who satisfied the criteria for authorship but are not listed. We further confirm that the order of authors listed in the manuscript has been approved by all of us.

We confirm that we have given due consideration to the protection of intellectual property associated with this work and that there are no impediments to publication, including the timing of publication, with respect to intellectual property. In so doing we confirm that we have followed the regulations of our institutions concerning intellectual property.

We further confirm that any aspect of the work covered in this manuscript that has involved either experimental animals or human patients has been conducted with the ethical approval of all relevant bodies and that such approvals are acknowledged within the manuscript.

We understand that the Corresponding Author is the sole contact for the Editorial process (including Editorial Manager and direct communications with the office). He/she is responsible for communicating with the other authors about progress, submissions of revisions and final approval of proofs. We confirm that we have provided a current, correct email address which is accessible by the Corresponding Author and which has been configured to accept email from biomaterials@elsevier.com.

Signed by all authors as follows:

Date

Ivan Lozić,

Richard V. Hartz, RHartz 14/5/2015

Carole A. Bartlett,

Jeremy A. Shaw,

Michael Archer,

Priya S.R. Naidu,

Nicole M. Smith,

Sarah A. Dunlop,

AUTHOR DECLARATION TEMPLATE

We the undersigned declare that this manuscript is original, has not been published before and is not currently being considered for publication elsewhere.

We wish to confirm that there are no known conflicts of interest associated with this publication and there has been no significant financial support for this work that could have influenced its outcome.

We confirm that the manuscript has been read and approved by all named authors and that there are no other persons who satisfied the criteria for authorship but are not listed. We further confirm that the order of authors listed in the manuscript has been approved by all of us.

We confirm that we have given due consideration to the protection of intellectual property associated with this work and that there are no impediments to publication, including the timing of publication, with respect to intellectual property. In so doing we confirm that we have followed the regulations of our institutions concerning intellectual property.

We further confirm that any aspect of the work covered in this manuscript that has involved either experimental animals or human patients has been conducted with the ethical approval of all relevant bodies and that such approvals are acknowledged within the manuscript.

We understand that the Corresponding Author is the sole contact for the Editorial process (including Editorial Manager and direct communications with the office). He/she is responsible for communicating with the other authors about progress, submissions of revisions and final approval of proofs. We confirm that we have provided a current, correct email address which is accessible by the Corresponding Author and which has been configured to accept email from biomaterials@elsevier.com.

Signed by all authors as follows:

Date

Ivan Lozić,

Richard V. Hartz,

Carole A. Bartlett,

Jeremy A. Shaw, 12/5/15

Michael Archer,

Priya S.R. Naidu,

Nicole M. Smith,

Sarah A. Dunlop,

AUTHOR DECLARATION TEMPLATE

We the undersigned declare that this manuscript is original, has not been published before and is not currently being considered for publication elsewhere.

We wish to confirm that there are no known conflicts of interest associated with this publication and there has been no significant financial support for this work that could have influenced its outcome.

We confirm that the manuscript has been read and approved by all named authors and that there are no other persons who satisfied the criteria for authorship but are not listed. We further confirm that the order of authors listed in the manuscript has been approved by all of us.

We confirm that we have given due consideration to the protection of intellectual property associated with this work and that there are no impediments to publication, including the timing of publication, with respect to intellectual property. In so doing we confirm that we have followed the regulations of our institutions concerning intellectual property.

We further confirm that any aspect of the work covered in this manuscript that has involved either experimental animals or human patients has been conducted with the ethical approval of all relevant bodies and that such approvals are acknowledged within the manuscript.

We understand that the Corresponding Author is the sole contact for the Editorial process (including Editorial Manager and direct communications with the office). He/she is responsible for communicating with the other authors about progress, submissions of revisions and final approval of proofs. We confirm that we have provided a current, correct email address which is accessible by the Corresponding Author and which has been configured to accept email from biomaterials@elsevier.com.

Signed by all authors as follows:

Date

Ivan Lozić,

Richard V. Hartz,

Carole A. Bartlett,

Jeremy A. Shaw,

Michael Archer,

Priya S.R. Naidu,

Nicole M. Smith,

Sarah A. Dunlop, May 6th 2015.

AUTHOR DECLARATION TEMPLATE

K. Swaminathan Iyer, 12/5/15

Matt R. Kilburn 13/5/15

Melinda Fitzgerald Melinda Fitzgerald Digitally signed by Melinda Fitzgerald DN: cn=Melinda Fitzgerald, o=Experimental and Regenerative Neurosciences, ou=School of Animal Biology, email=lindy.fitzgerald@uwa.edu.au, c=AU Date: 2015.05.05 17:05:38 +08'00'

[LIST AUTHORS AND DATED SIGNATURES ALONGSIDE]

THE UNIVERSITY OF WESTERN AUSTRALIA
Achieving International Excellence

School of Animal Biology,
Experimental and Regenerative Neurosciences,
The University of Western Australia,
M317, Crawley, 6009, WA, AUSTRALIA
T 61 8 6488 2353
F 61 8 6488 7527
E lindy.fitzgerald@uwa.edu.au

29th September, 2015

Editor in Chief: Biomaterials
Prof K.W. Leong
Columbia University, New York,
NY, USA

Dear Prof Leong,

Thank you for considering a revision of our manuscript entitled "Enabling Dual Cellular Destinations of Polymeric Nanoparticles for Treatment Following Partial Injury to the Central Nervous System" by Ivan Lozić, Richard V. Hartz, Carole A. Bartlett, Jeremy A. Shaw, Michael Archer, Priya S.R. Naidu, Nicole M. Smith, Sarah A. Dunlop, K. Swaminathan Iyer, Matt R. Kilburn and Melinda Fitzgerald for publication in *Biomaterials*.

We have considered the Reviewer's comments carefully and made alterations in response to each suggestion, described as follows:

Reviewer #2: The authors report…. The paper is very well drafted but Figure 1 should be revised. Nanoparticle synthesis should be explained a bit more in detail. a successful antibody binding is very depending on concentration and the efficacy is quite low. Furthermore the size of the nanoparticle is increasing, it is not much of a problem here but I was wondering if the antibody cannot be replace by a peptide. In other words is an antibody the only option to facilitate this uptake and effect. Otherwise it is a beautiful paper with high profile work and should be published after minor revisions.

The Reviewer has made a series of suggestions and comments regarding the data described in Figure 1. It is possible that the Reviewer did not see the comprehensive description of Nanoparticle synthesis in the section of that name in the Materials and Methods part of the manuscript (page 6). The section refers to previously published work describing further details of nanoparticle synthesis, fully describes the procedures followed in the current work and also includes the ^{1}H-NMR analysis. We have now referred the reader to these sections in the revised manuscript. It is also worth noting that additional DLS NP characterisation data are provided in Table 1. As such, we respectfully suggest that no further revision of Figure 1 is required.

The Reviewer correctly notes that successful antibody binding depends upon the concentration of antibody. However it is noteworthy that our preparation protocol uses 5:1 mass ratio of NP to antibody, which does not result in use of particularly large amounts of antibody. We have also demonstrated successful antibody linkage to NP in Figure 1C. Significant and substantial differential efficacy of the antibody linked NP is demonstrated in the data of Figures 5U, 5X and 7J.

The Reviewer suggests replacing the antibody with a peptide. Antibodies allow the specific targeting of NP to antigens on the surface of cells. Their three dimensional and complex conformational structure allow specific interactions to occur. While specific interactions may also be facilitated by peptides, metabolic instability due to enzymatic degradation and peptides would need to be overcome. We have added further information regarding our choice of antibodies to the revised manuscript, in response to the Reviewer's comments.

Reviewer #5: Of a great disappointment, the work in in its second part, showed to be descriptive; lacking any mechanistic element to assess astrocytic/neuronal injury. The first part of the work ie

characterization of NP- with state of the art approaches is excellent, however the second part failed dramatically as the authors didn't have any well-defined Neural Injury indices that can show neuroprotection, ie it is the main aim of such NP-AQP approach.

The current study is focussed on characterizing the interaction of various NP formulations with specific cell types and the functional effect of these interactions. As such, the outcome measures for the experiments in the second part of the study describe the identification of cell types, co-localisation of NPs with various functionalities with these cells, and a suite of oxidative stress based outcome measures as well as novel NanoSIMS assessment of calcium microdomains. The oxidative stress measures are particularly relevant given the encapsulation of the anti-oxidant resveratrol within the NP.

We appreciate the Reviewer's point regarding the potential inclusion of indices of neuronal death or neuroprotection. Indeed we have already published a number of articles characterising necrotic and apoptotic death of the key neuronal cells, retinal ganglion cells, following partial injury to the optic nerve (Fitzgerald et al 2009, IOVS). However, we have also demonstrated that preservation of retinal ganglion cell numbers does not always correlate to all-important functional outcomes (Savigni et al 2013 Neuropharmacology). As such, given the large volume of data already presented in the manuscript, we chose to focus on the key outcomes of oxidative stress and function that clearly demonstrate cell localisation and efficacy of our nanoparticle therapeutic system. Nevertheless, we appreciate the validity of the Reviewer's point and have added our rationale for choice of outcome measures to the revised manuscript, at the beginning of the section describing functional outcomes.

Major comments:

1- the authors need to characterize neural injury levels and mechanism ie apoptotic vs necrotic injury, the use of spectrin break down via western blotting is an easy approach that can answer this question among the different groups of the in vitro and in vivo cohorts. (Refer to the work of Hayes, Wang and Pike for spectrin); alternatively tunnel assay + MTT LDH need to be performed...I mean with all the first part and its tremendous effort, LDH and MTT could be easily performed to assess injury and protection.

We refer the Editor to our response to the previous comment by Reviewer #5. In addition it is worth noting that the MTT assay needs to be performed on live cells and as such cannot be effectively used on the cryopreserved *in vivo* tissue of the current study. It is an *in vitro* based assay. The LDH assay is also only really informative on live tissue, enabling assessment of enzyme activity, and would require an entire new cohort of animals to collect fresh frozen tissue samples. While these experiments could be done, it is not clear that they would substantially add to the assessment of oxidative stress and metabolism we have already performed. Our assessments of 8OHDG for DNA oxidative damage as well as AQP4 immunoreactivity and calcium microdomains provide similar outcomes to those suggested by the reviewer. The volume of data that we have presented in the current manuscript is already substantial and we respectfully submit that it is appropriate to answer the specific questions we have proposed. The core finding of the current manuscript is that it is essential to comprehensively investigate NP location, interactions and effects, both *in vitro* and *in vivo*, in order to work towards full understanding of functional outcomes. We have conducted these comprehensive investigations and in our opinion, the proposed additional experiments would not change the fundamental outcome of the study.

2- some proper control are lacking, NP-AQP AB treated with anti-anti AQP need to be studied to show that if you neutralize the AQP antibody there is no effect on injury. Cell culture need to be treated with naked resveratrol as well.

The use of one antibody to attempt to neutralise the effects of a second antibody is limited by the locations of antibody epitopes and would provide equivocal outcomes. Accordingly, in preference to the approach suggested by the reviewer, we have included the control preparation of NP with the MHA linker but no AB (NP-MHA), and compared this preparation to NP-MHA-AB in the data provided in Figures 1 and 3, in order to provide an appropriate control for the presence of antibody.

We were not able to include the NP-MHA control in the *in vivo* studies due to the limitations on sample numbers able to be assessed using the NanoSIMS technique (as described in full in the Materials and Methods section). However the NP-MHA-Res control, which gave significantly different outcomes to NP-MHA-Res-AB (Figures 5U, 5X and 7J), serves as an effective control in the *in vivo* context.

We refer the reviewer to Supplementary Figure 1 (now Figure 1 of the associated Data in Brief article), which already contains a comparison of NP containing resveratrol to naked resveratrol (the equivalent concentration of resveratrol not encapsulated in NP). Resveratrol encapsulated in NP was more effective at reducing an oxidative stress indicator than the naked resveratrol; the inclusion of this control has now been specifically noted in the revised manuscript.

3- the number of animals for behavioural assessment needs to be revisited

We acknowledge that the number of animals used for the behavioural assessments is relatively low. Nevertheless a significant difference between groups was observed by investigators blinded to group identity. Analysis of a new cohort of animals with larger numbers is unlikely to change an already significant result. It is not possible for us to add animals to the existing analysis as all animals need to be injected with NPs prepared at the same time in order to allow statistical comparison between groups. As requested by the reviewer, we have now revisited this issue in the Materials and Methods section of the revised manuscript.

4-the title and the use of neurotrauma NEED to be changed... Neurotrauma is a spectrum of disorders including brain injury (traumatic, etc), and spinal cord injury etc....By itself it is not a unique disorder. Of interest, partial model. the optic nerve transection is far from a neurotrauma process and is far from being a true Neurotrauma

As requested, we have changed the title. Given that the optic nerve is part of the central nervous system, the revised title is “Enabling Dual Cellular Destinations of Polymeric Nanoparticles Following Treatment of Partial Injury to the Central Nervous System”.

5- there is no rationale why glutamate is added, for audience in NP, they won’t recognize what is the addition of glutamate may induce, and also there is no correlation provided to the readers how this glutamate excitotoxicity mimics partial optic nerve transection. Please add this in the Intro.

We thank the Reviewer for pointing out the lack of background on use of glutamate as a model of CNS injury and have added this information to the Introduction of the revised manuscript as requested.

Minor

the whole abstract need to be rewritten with its wrong wordings and sentence structure. It seems different authors wrote the abstract from the rest of the manuscript. they seem so disconnected.

We have revised the abstract as requested, following the flow of information of the Results and Discussion more closely.

Overall, the manuscript is a technical report that has two components: 1- nanoparticles conjugation to aquaporin antibody using different state of the art techniques and thee authors fulfilled this task successfully. In aim 2 where they want to assess this conjugation, they kept using the term neurotrauma showing that the antioxidant resveratrol has an effect. The second task, being the major finding of this work is poorly developed and is more descriptive with no in depth assessment of how these NP treatment affect cellular injury..... NO mechanistic contribution.

Unless they are able to provide these experiments in future submission, this work is not sufficient to be published.

This issue has largely been addressed in responses above. To conclude, we consider that the mechanistic understanding provided by the oxidative stress measures, AQP4 assessments, calcium microdomain quantification using novel NanoSIMS, together with comprehensive assessments of NP localisation within a broad range of cell types utilising fluorescence microscopy, NanoSIMS and electron microscopy provides substantial mechanistic understanding. We demonstrate the mechanism by which our NP are likely having positive effects on function, *via* localisation of the NP within macrophages and reducing oxidative stress that arises from these cells. Further experiments assessing neuroprotection would be assessing a mechanism secondary to the primary effects on macrophages and would in our opinion be of limited benefit. Our published work, to which we now refer in the revised manuscript, provides further evidence that it is function that is important and further experiments assessing apoptosis and necrosis would not provide direct mechanistic insight.

We believe that we have addressed the concerns of the reviewers as appropriate and hope you will view our revised submission favourably. Thank you for your time and consideration.

Yours sincerely,

Melinda Fitzgerald, PhD

Enabling Dual Cellular Destinations of Polymeric Nanoparticles for Treatment Following Partial Injury to the Central Nervous System

Lozić, I.,[1, 2] *Hartz, R.V.,*[2] *Bartlett, C.A.,*[2] *Shaw, J.A.,*[3] *Archer, M.,*[2] *Naidu, P.S.R,*[1, 2] *Smith, N.M.,*[1, 2] *Dunlop, S.A.,*[2 ł] *K. Swaminathan Iyer,*[1 ł]*Kilburn, M.R.,*[3] **Fitzgerald, M.*[2]

[1]School of Chemistry and Biochemistry, [2]Experimental and Regenerative Neurosciences, School of Animal Biology, [3]Centre for Microscopy, Characterisation and Analysis, The University of Western Australia, 35 Stirling Hwy, Crawley WA 6009, Australia

[ł]equal contribution

*Corresponding Author: Melinda Fitzgerald

Email: lindy.fitzgerald@uwa.edu.au; Fax: +61 8 6488 7527; Tel: +61 8 6488 2353

ABSTRACT

Following neurotrauma, oxidative stress is spread *via* the astrocytic syncytium and is associated with increased aquaporin 4 (AQP4), inflammatory cell infiltration, loss of neurons and glia and functional deficits. Herein we evaluate multimodal polymeric nanoparticles functionalized with an antibody to an extracellular epitope of AQP4, for targeted delivery of an anti-oxidant as a therapeutic strategy following partial optic nerve transection. Using fluorescence microscopy, spectrophotometry, correlative nanoscale secondary ion mass spectrometry (NanoSIMS) and transmission electron microscopy, *in vitro* and *in vivo*, we demonstrate that functionalized nanoparticles are coated with serum proteins such as albumin and enter both macrophages and astrocytes when administered to the site of a partial optic nerve transection in rat. Antibody functionalized nanoparticles synthesized to deliver the antioxidant resveratrol are effective in reducing oxidative damage to DNA, AQP4 immunoreactivity and preserving visual function. Non-functionalized nanoparticles evade macrophages more effectively and are found more diffusely, including in astrocytes, however they do not preserve the optic nerve from oxidative damage or functional loss following injury. Our study highlights the need to comprehensively investigate nanoparticle location, interactions and effects, both *in vitro* and *in vivo*, in order to fully understand functional outcomes.

KEYWORDS Polymer nanoparticles; Central nervous system injury; oxidative stress and aquaporin4; targeted drug delivery of antioxidants; nanoscale secondary ion mass spectroscopy (NanoSIMS); macrophages

INTRODUCTION

Structural and functional losses following neurotrauma are exacerbated by the spread of injury beyond the initial insult. This secondary degeneration is thought to be triggered by glutamate excitotoxicity[1, 2] and calcium ion (Ca^{2+}) overload,[3] leading to oxidative stress.[4] Oxidative stress during secondary degeneration is associated with astrocyte hypertrophy, immune cell infiltration, loss of neurons and glia, structural abnormalities in myelin and chronic functional deficits.[5-7] Hitherto, strategies for limiting oxidative stress induced by neurotrauma have utilized antioxidants,[8, 9] receptor antagonists or ion channel inhibitors to interrupt the biochemical cascades that lead to oxidative stress.[10, 11] Resveratrol is an example of an antioxidant that has shown promising protective results *in vitro* and *in vivo*,[12-15] attenuating neuronal swelling whilst increasing recovery of normal neuronal morphology,[16] and improving locomotor responses following percussion-induced neurotrauma in young Wistar albino rats.[17] However, *in vivo* trials have shown that in addition to poor solubility in water (30 ng/mL), resveratrol has low bioavailability and is rapidly metabolized following administration.[18, 19] As such, despite promising *in vitro* results, therapeutic strategies such as resveratrol have thus far not been a clinical success, and no effective treatments currently exist to prevent the spread of pathology following injury to the central nervous system (CNS). [20, 21] Novel nanosystems have considerable potential for the treatment of currently intractable diseases and injuries, including neurotrauma. Nanoparticle systems provide a way to overcome issues including poor bioavailability[22, 23] and toxicity at required doses,[20, 24] which have plagued traditional treatments. Engineered polymer nanoparticles are non-toxic,[25] can encapsulate therapeutic agents and may deliver them to a specific target with the aid of a targeting moiety,[26-30] thereby potentially overcoming poor bioavailability and off-target side-effects.

Astrocytes are thought to contribute substantially to the spread of oxidative stress *via* the movement of excess Ca^{2+} and reactive species through the astrocytic syncytium.[31, 32] We and others have previously demonstrated up-regulation of the plasma membrane bound water channel AQP4 in CNS tissue affected by neurotrauma,[33, 34] particularly in astrocytes.[34] Therefore, AQP4 can be exploited as a potential target to direct nanoparticles functionalized with antibodies recognizing an extracellular epitope of this protein, to astrocytes. Here we use an *in vitro* model of injury to the CNS, and demonstrate similar increases in AQP4 in mixed retinal cells. Glutamate is added to the cultures to simulate the glutamate excitotoxicity that occurs following injury to neurons and supporting glia[35] resulting in increased AQP4 immunoreactivity. *In vivo*, infiltration of microglia and macrophages[36, 37] further contribute to the spread of reactive species and resultant oxidative stress;[32, 38, 39] hence targeting of nanoparticles to infiltrating inflammatory cells is also likely to be beneficial. The tracking of targeted nanoparticles, their therapeutic cargoes and their effects on cells in tissue *in vivo* can be problematic. We have developed multimodal polymeric nanoparticles that encapsulate smaller magnetite nanoparticles and contain fluorescent dyes, thereby allowing them to be imaged *in vivo*.[40] However, the therapeutic payload can be much more difficult to track. The use of stable-isotopes (e.g. ^{13}C, ^{15}N or ^{127}I) in therapeutic agents has allowed for tracking of anti-cancer drugs using nanoscale secondary ion mass spectrometry (NanoSIMS) in tumors,[41-43] with individual cell types identified using fluorescence microscopy.[44, 45] The presence of concentrated deposits of iron in the form of Fe_3O_4 (magnetite) can also be used to track the nanoparticles using NanoSIMS. We have previously used NanoSIMS in conjunction with fluorescence immunohistochemistry[46] to characterize changes in the distribution of Ca microdomains *in vivo*, following partial optic nerve transection injury. Here, we leverage the spectral and spatial resolution of NanoSIMS,[47] to

simultaneously investigate the localization of nanoparticles and the therapeutic agent resveratrol encapsulated within them, as well as assess physiologically relevant outcomes of nanoparticle treatment on Ca microdomain dynamics *in vivo*. We combine NanoSIMS outcomes with fluorescence microscopy and transmission electron microscopy (TEM), to demonstrate that functionalizing antioxidant loaded nanoparticles with the anti-AQP4 antibody causes these nanoparticles to associate with both astrocytes and macrophages, resulting in reduced oxidative damage and preserved function *in vivo*.

MATERIALS AND METHODS

Materials

All chemicals and materials were purchased from Sigma-Aldrich unless otherwise stated: poly(glycidyl methacrylate) (PGMA, donated by Igor Luzinov, University of North Carolina); rhodamine-B (RhB, Fluka Chemika AG); 6-maleimidohexanoic acid (MHA), *tris*(2-carboxyethyl)phosphine hydrochloride (TCEP·HCl), methyl ethyl ketone (MEK, Fisher Chemical); diethyl ether, chloroform (Merck Millipore); benzyl ether, resveratrol, ^{13}C Resveratrol, $Fe(acac)_2$, 1,2-tetradecanediol, oleic acid, oleylamine, pluronic F-108, MACS® separation columns (Miltenyi Biotec); rare-earth magnets (Aussie Magnets); bovine serum albumin (BSA). Tissue culture and immunohistochemistry reagents: Dulbecco's modification of Eagles Medium (DMEM, high glucose, containing L-glutamate and pyruvate), penicillin/streptomycin, poly-L-lysine, fetal bovine serum, GlutaMAX 100×, trypsin/EDTA, Hoechst nuclear dye (all from Gibco, Life Technologies); glutamate (Sigma Aldrich); DCFH-DA

(Thermo Scientific); polyclonal anti-AQP4 (Alamone labs), anti-βIII tubulin (Covance), anti carboxymethyl lysine (anti-CML, Cosmo Bio), anti-GFAP (Sigma), anti-8OHdG (Abcam), anti-ED1 (Millipore) antibodies; AlexaFluor (AF) 488, AF555 and AF647 (Life Technologies) secondary antibodies; Fluoromount-G (Southern Biotech). Custom made monoclonal antibodies directed against the extracellular epitope of AQP4 (YTGASMNPARSFGPAVIMGNWENHWIC) was generated by Dr K Davern (Monoclonal Antibody Facility, Harry Perkins institute of Medical Research, Western Australia).

Nanoparticle synthesis

Fe_3O_4 magnetite nanoparticles were synthesized in accordance with established procedures.[48] Polymer based nanoparticles (NPs) were prepared as described,[49] with the following modifications. PGMA (500 mg, M_w 120,000 g/mol) was refluxed in MEK for 18 hours with MHA (736.7 mg, 3.49 mmol). The resulting white product (PGMA-MHA) was isolated from Et_2O, and allowed to dry at room temperature for 1 hour. Proton nuclear magnetic resonance (NMR) of PGMA-MHA indicated the presence of maleimide olefin protons at 6.68 ppm, confirming MHA attachment to PGMA. ^{1}H-NMR (400 MHz, $CDCl_3$): δ 6.68 (s, maleimide olefin), 4.06 (d, J = 195 Hz, 2H), 3.23 (s, 1H), 2.74 (d, 83 Hz, 2H), 1.96 (m, 2H), 1.05 (m, 3H) ppm. Following this, all of the product was placed in MEK with RhB (55.0 mg, 0.12 mmol) and refluxed for 18 hours. The resulting pink/red product (PGMA-MHA-RhB) was isolated from Et_2O. ^{1}H-NMR of PGMA-MHA-RhB indicated the presence of peaks in the aromatic region corresponding to that of RhB. ^{1}H-NMR (400 MHz, $CDCl_3$): δ 8.33 (dd, 1.6 Hz, 6.8 Hz), 7.66 (m), 7.18 (m), 7.07 (d, 9.2 Hz), 6.74 (d, 9.2 Hz), 6.68 (s, maleimide olefin), 4.06 (d, J = 195 Hz, 2H), 3.23 (s, 1H), 2.74 (d, 83 Hz, 2H), 1.96 (m, 2H), 1.05 (m, 3H) ppm. Product was kept in

chloroform until needed. For synthesis of NP containing no maleimide linker, the MHA attachment step was omitted.

Antioxidant containing multimodal NP were synthesized using the following procedure. PGMA-MHA-RhB was dissolved in MEK (4.5 mL) along with resveratrol (15 mg, 65.7 μmol), to which was added Fe_3O_4 magnetite nanoparticles (10 mg, 43.2 μmol) in $CHCl_3$ (1.5 mL). This mixture was added drop-wise to a vigorously stirring aqueous solution of Pluronic F-108 (12.5 mg/mL). The resulting emulsion was homogenized with a probe-type ultrasonicator for 2 min at low power and stirred overnight under a slow flow of $N_{2(g)}$ to evaporate the solvents. The emulsion was then centrifuged at 3000 g for 45 min and the supernatant passed through a magnetic separation column. The collected NP were washed from the column, collected in Pluronic F-108 (2.5 mg/mL) and stored at 4 °C until use. Control NP were generated by omitting resveratrol or MHA addition steps from the procedure. For *in vivo* experiments, ^{13}C-enriched resveratrol (99 atom % ^{13}C for 6 of the 14 C) was used with no other modification to the synthesis, in an attempt to track the release of resveratrol using NanoSIMS.

NP compositions synthesized and referred to in this text are as follows: PGMA-RhB with no resveratrol (NP-e); PGMA-RhB encapsulating resveratrol (NP-Res); PGMA-MHA-RhB with no resveratrol (NP-MHA); PGMA-MHA-RhB encapsulating resveratrol (NP-MHA-Res); PGMA-MHA-RhB functionalized with anti-AQP4 antibody with no resveratrol (NP-MHA-AB); PGMA-MHA-RhB functionalized with anti-AQP4 antibody and encapsulating resveratrol (NP-MHA-Res-AB).

NP characterization

NP size was determined using Dynamic Light Scattering together with zeta potential determination (DLS, Malvern ZetaSizer Nano), and NP size visualized using transmission electron microscopy (TEM, JEOL 2000FX; JEOL, Japan), using dried suspensions of NP. NP resveratrol content was determined by high performance liquid chromatography (HPLC) as follows. To facilitate the release of resveratrol from NPs, a known mass of freeze-dried NP was suspended in a defined volume of MeOH (1 mL) and sonicated for 1 hour, allowed to sit for 1 hour at ambient temperature and pressure, followed by centrifugation at 16873 RCF for 30 mins. 90 μL of the supernatant was removed, run through a reverse-phase column (Phenomenex Luna 5 μm C18(2) 100 Å) maintained at 25 ˚C and analyzed using a Waters 2695 Separation Module connected to a Waters 2489 UV/Vis detector ($\lambda_{detection}$ = 304 nm). The mobile phase was composed of 1.25 % CH_3COOH in a 20:80 mixture of MeCN and milliQ-H_2O (flow rate = 10 ml/min).

Release of resveratrol from NP was measured in phosphate buffered saline (PBS) at pH 6 (to mimic acidic conditions following injury) and 7 (to mimic physiological conditions). 1 mg of NP (NP-MHA±Res) was suspended in 1 mL of PBS (the 'reservoir' or 'sink') and incubated at ambient temperature and pressure. At 30 min intervals for 360 min, the preparation was centrifuged at 16873 RCF for 5 min and 90 μL samples of supernatant taken for HPLC analysis, as described above. The remainder of the supernatant was discarded, with care taken not to disturb the NP pellet. The NP pellet was re-suspended in 1 mL of fresh PBS for each subsequent 30 min incubation.

Functionalisation of NP with anti-AQP4 antibodies

A series of custom-made anti-extracellular AQP4 monoclonal antibodies were screened for immunoreactivity to rMC1 retinal Müller cells (gift from Dr. Gabriel A. Silva, University of San Diego, CA) that had been cultured for 24 hr according to established conditions[49] in DMEM (high glucose, containing l-glutamate) medium supplemented with fetal bovine serum (heat inactivated, 10 % v/v), penicillin/streptomycin (1 % v/v [50 μm/L, 50 μg/mL]) and GlutaMAX 100× (1 % v/v) at 1×10^5 cells/mL. Immunoreactivity was assessed as described[49] using a 1:3 dilution of sera on cells fixed in paraformaldehyde (4 %), and visualized with AF448 secondary antibodies. Secondary antibody-only controls were included and images were captured by confocal microscopy (Leica TCS SP2; Leica Microsystems, Germany). The anti-AQP4 monoclonal antibody with the greatest immunoreactivity to rMC1 cells (1A6) was chosen for further studies. Anti-AQP4 antibody (0.1 mg/mL) was reacted with TCEP (0.04 mmol/L) in degassed PBS at 37 °C under $N_{2(g)}$ for 2 hours to reduce the disulfide bonds from cysteine groups on the antibody in order to facilitate reaction of the thiols with the maleimide olefin of MHA. Aliquots of prepared antibody were transferred to stirring suspensions of NP to give a reaction volume with a 5:1 mass ratio of NP to antibody. Following stirring at 37 °C under $N_{2(g)}$ for 2 hours, the resulting mixture was centrifuged in 1.5 mL aliquots at 16873 RCF for 30 mins, and the supernatant discarded. The washing process was repeated 3 times to ensure removal of unattached antibody and the resulting NP-antibody pellet was re-suspended in PBS at appropriate concentrations for *in vitro* and *in vivo* experiments. Unreacted maleimide functional groups were not blocked following antibody coupling reaction. Attachment of anti-AQP4 antibodies to NP was confirmed via incubation of NP with species appropriate AF488 secondary antibodies (1/500) at 37 °C under $N_{2(g)}$ for 2 hours and assessment of fluorescence using an EnSpire Multimode Plate Reader (Perkin Elmer, USA). The interaction of NP with albumin was assessed

by suspending 200 μg of various NP preparations in 500 μL of albumin (6.0 mg/mL) and incubating for 24 hours at ambient temperature. Samples were centrifuged for 20 mins at 16873 RCF and three separate 2 μL samples of each supernatant assessed using a NanoDrop 2000 Spectrophotometer (ThermoFisher Scientific, USA) to determine the concentration of albumin in the remaining supernatant (absorption at 280 nm). The concentration of albumin remaining on NP preparations with and without resveratrol were also determined using the Nanodrop Spectrophotometer, subtracting the background absorbance of the NP alone, and expressing data in mg of albumin/ mg NP.

In vitro assessments of effects of NP

All procedures involving animals conformed to the National Health and Medical Research Council of Australia Guidelines on the Use of Animals in Research and were approved by the Animal Ethics Committee of The University of Western Australia (approval number RA3/100/1201). Primary mixed retinal cell cultures were prepared from Piebald Viral Glaxo (PVG) rat pups (<5 days postnatal) and cultured according to established procedures.[50] Cells were cultured for 48 hours in Neurobasal media (with 10 % fetal calf serum and 1 % glutamax) in wells pre-coated sequentially with 100 μL poly-L-lysine (10 μg/mL) and laminin (100 μg/mL). NP (200 μg/mL of NP; 10 μM of resveratrol) were added to cultures and incubated for a further 24 hours in the presence of glutamate (10 mM). Cells were washed, and incubated with 100 μL of DCFH-DA (100 μM) in cell culture media for one hour. Following removal of DCFH-DA, cells were solubilized in 100 μL of 0.1 % triton X100 solution and fluorescence assessed (EnSpire Multimode Plate Reader, $\lambda_{excitation}$ = 480 nm, $\lambda_{emission}$ = 530). Immunohistochemical analyses were conducted using established procedures,[51] on mixed retinal or rMC1 cells cultured

and treated with NP and/or glutamate as described above. Imaging was conducted on a Nikon Eclipse Ti inverted microscope (Nikon Corporation, Japan), with all images deconvoluted using autoquant blind deconvolution in Nikon Elements AT software. Representative single optical slices from within z-stacks were chosen for analysis and display. Contours were drawn around individual cells (using ImageJ/Fiji) and the immunoreactivity of these cells was assessed where appropriate, using ImageJ intensity analysis software.

In vivo assessments of effects of NP

Adult, female piebald viral Glaxo (PVG) black hooded rats (165–205 g, Animal Resource Centre, Murdoch, WA, Australia) were anaesthetized and partial optic nerve transection of the right optic nerve performed as described previously.[46] Animal treatment groups were normal (uninjured control), and animals that had undergone the partial optic nerve transection and were treated with PBS (vehicle), NP-MHA-Res, NP-MHA-AB or NP-MHA-Res-AB. All groups had an n = 4 animals: note that the number of animals per group was limited by the requirement for simultaneous processing for the key NanoSIMS outcomes and the size of freeze-substitution systems. The numbers of animals used per experimental group are in line with published studies conducted at the nano and ultrastructural scale.[6, 7, 52] Additionally, the outcomes were assessed by investigators blinded to group identity and statistically significant outcomes were observed. The nature of fine scale analyses such as NanoSIMS and TEM assessments of ultrastructure necessitate analysis of a relatively small number of animals, compensated at least in part by analysis of multiple fields of view for each analysis to ensure random sampling. Note that a sham injury group was not included as we have previously demonstrated no statistical differences between sham injured and normal optic nerve, when assessing a range of relevant outcome

measures.[37] At the time of injury, 0.25 µl of NP preparations at 5 µg/ml were injected directly into the injury site using a Nanojet (World Precision Instruments). Nanoparticles used in *in vivo* testing contained a resveratrol payload of 5.5 µg (0.024 µmol) per mg of nanoparticle. Prior to harvesting of optic nerve tissue at 24 hours after injury, the optokinetic nystagmus visual reflex was assessed as described previously.[53] Visual function was confined to the injured optic nerve, as left eyelids of all animals, including normal control animals, were sutured shut at the time of injury. Optic nerve samples were prepared for NanoSIMS using rapid cryopreservation by high pressure freezing, followed by freeze substitution and resin infiltration as described previously.[46, 54] Adjacent sequential sections to those prepared for NanoSIMS analysis were assessed immunohistochemically and for RhB fluorescence, as described for *in vitro* assessments. Quantification of ED1+ cells containing NP was conducted by counting all ED1+ cells in a single optic nerve section at the injury site from each animal and expressing data as a proportion of ED1+ cells containing NP. 8OHdG and AQP4 immunointensity was quantified using ImageJ analysis software to determine the area or mean intensity above an arbitrarily defined and constant threshold intensity in a single optic nerve section at the injury site from each animal. Additional tissue sections (0.2 µm thick) were prepared and imaged using TEM (JEOL 2100; JEOL, Japan).

Sections selected for NanoSIMS analysis were assessed using the same criteria as described previously[46]. In brief: secondary ion micrographs were acquired using the CAMECA NanoSIMS 50 ion microprobe at The University of Western Australia. Several sections per optic nerve were analyzed, with at least two fields of view assessed per section. To afford a steady state of secondary ion yield all fields of view were implanted with a primary ion dose of 1×10^{17} ions/cm^2 prior to imaging. Each field of view (FOV) was imaged three times, to determine (i)

structure, (ii) ^{13}C content and (iii) Ca and Fe distributions. For (i) and (ii), a Cs^+ primary ion beam (nominal beam diameter = 100 nm, current = 1.5 pA) was used to sputter the negative ion species $^{12}C^{12}C^-$, $^{12}C^{14}N^-$, $^{31}P^-$, $^{32}S^-$, $^{35}Cl^-$ and secondary electrons (for structural information), as well as $^{12}C^-$, $^{12}C^{12}C^-$, $^{13}C^{12}C^-$, $^{12}C^{14}N^-$, $^{31}P^-$ and secondary electrons (for ^{13}C isotopic information). For (iii), an O^- primary ion beam (nominal beam diameter = 600 nm, current = 28 pA) was then used to sputter the positive ion species $^{12}C^+$, $^{23}Na^+$, $^{40}Ca^+$, $^{56}Fe^+$ and $^{133}Cs^+$. The Cs signal is derived from the implanted Cs primary ion, and can be used for relocating the exact FOV and tuning the secondary ion optics. All FOV were 30 × 30 μm in dimension, and imaged at a resolution of 256 × 256 pixels, with a dwell time of 30 ms/pixel. The size of the FOV was verified using a 10 μm Cu grid. For ^{13}C analysis, there was significant isobaric interference on mass 25. As such, the instrument was tuned for high mass resolution. Charge build-up during Cs^+ primary beam use was not observed. Adequate sample conductivity was provided by the combination of underlying Si substrate and overlying Au coat provided. As the valency of the detected ions is not discernible, detected ions are referred to by their isotopic species (e.g. ^{40}Ca) and elemental symbol (Ca), not oxidation state (e.g. Ca^{2+}). During collection of ^{13}C data, FOV from normal uninjured control animals with no ^{13}C-enriched resveratrol were imaged at the commencement and completion of each imaging session.

Analysis of Ca microdomains using NanoSIMS was conducted using the OpenMIMS plugin for Fiji/ImageJ (version 2.0; NIH)[55] as described previously.[46] In brief, microdomain density (defined as the number of microdomains in a given area, in a particular tissue type) and microdomain proportion (defined as the area of microdomain in a given area, in a particular tissue type) were determined (all in μm^2) for each FOV in a section, and data were averaged for all FOV for a particular animal. Tissue type was determined as described previously:[46] in brief,

secondary ion maps for $^{31}P^-$, $^{32}S^-$ and $^{12}C^{14}N^-$ were assigned to color channels in RGB images (referred to as P-S-CN images) and aligned with immunohistochemically assessed adjacent sections, using GFAP to indicate astroglial regions, or AQP4. We have previously demonstrated, using immunohistochemical assessment of GFAP, βIII-tubulin and myelin basic protein, that features in P-S-CN images facilitate identification of tissue type.[46] Note that due to the wide emission spectrum of RhB in the NP, immunohistochemical analyses were limited to use of AF488 secondary antibodies. Therefore, axonal regions were defined as areas not immunopositive for GFAP, as described previously.[46]

Analysis of ^{13}C content using NanoSIMS was conducted on three types of regions of interest (ROI): specific hotspots of Fe signal observed in tissue from animals treated with NP; the surrounding tissue (non-Fe hotspot) and across the whole FOV. ROIs corresponding to Fe hotspots were generated from $^{56}Fe^+$ bitmaps, with data extracted from both $^{13}C^{12}C^-$ and $^{12}C^{12}C^-$ bitmaps. Bitmaps were generated using a method derived from the Ca microdomain NanoSIMS analyses described previously.[46] Individual grey values were applied to each ROI (RGB color model values: hotspots = 141414, non-Fe hotspot tissue = 323232). $^{13}C/^{12}C$ ratios for each ROI were determined by halving the result from dividing the total $^{13}C^{12}C^-$ count by the $^{12}C^{12}C^-$ count, to account for using the double ion species (which has a higher ion yield than the single ion species, $^{12}C^-$ and $^{13}C^-$). The $^{13}C/^{12}C$ ratios of all ROIs were converted to atomic percent (^{13}C %) using the following formula:

$$^{13}\mathrm{C}\ \% = \left(\frac{R}{1+R}\right), \text{ where } R = 0.5\left(\frac{total\ ^{13}\mathrm{C}^{12}\mathrm{C}\ ion\ count}{total\ ^{12}\mathrm{C}^{12}\mathrm{C}\ ion\ count}\right)$$

where total ion count is for the chosen ROI. ^{13}C enrichment was visualized as a $^{13}C^{12}C/^{12}C^{12}C$ ratio HSI, where ratio is represented by a color scale where the minimum was set to natural

abundance (scale ratio factor = 10,000, max = 500, min 207). Enrichment was determined by comparison to signal collected in non-enriched control FOV.

Statistical analyses

Significances were determined with SPSS statistical software using Student's t-test or one-way ANOVA as appropriate, and Bonferroni, Dunnett's or Games-Howell *post-hoc* tests for *in vitro* assessments and Kruskal-Wallis tests for *in vivo* measures: $P \leq 0.05$ was regarded as significant.

RESULTS AND DISCUSSION

Synthesis and characterization of multifunctional polymeric nanoparticles

In this work, we have prepared multimodal polymeric nanoparticles (NP) containing the antioxidant resveratrol. NPs were synthesized from poly(glycidyl methacrylate) (PGMA): we have shown that our PGMA NP are non-toxic, stable under physiological conditions and readily functionalizable *via* the epoxide group.[40, 49, 56] We have functionalized the NP with antibodies to an extracellular epitope of AQP4, to facilitate targeting to astrocytes following injury to the CNS. The complex, folded protein structure of an antibody results in an interaction with the target antigen that is specific, high affinity and relatively resistant to enzymatic degradation. In order to generate the fully functionalized NP, a multi-step synthesis procedure was followed, with characterization throughout. Prior to synthesis of NP, the PGMA backbone was functionalized with maleimide groups using 6-maleimidohexanoic acid (MHA), to enable binding of the anti-AQP4 antibody (Figure 1a). MHA attachment to PGMA (PGMA-MHA) was confirmed using ^{1}H-NMR, by the presence of a singlet at δ 6.68 ppm corresponding to the olefin

protons on MHA (for further details see the NP synthesis and NP characterization sections in the Materials and Methods). PGMA-MHA was further functionalized with the fluorescent dye Rhodamine B (RhB), as reported previously,[49] and confirmed via ^{1}H-NMR. Dry functionalized PGMA-MHA with RhB was used to synthesize NP containing magnetite, with or without resveratrol, using spontaneous emulsification.[49] The size of the resultant NP was ~ 150 nm, as determined using DLS (specific SI size distributions listed in Table 1); the data describe single narrow peaks, indicating that the NP exist as distinct individual particles in solution. NP were purified and antibodies attached (Figure 1b), resulting in a marked increase in total NP diameter but no observable change in zeta potential (Table 1). Antibody attachment to NP was confirmed by incubating the NP preparations with a fluorescent secondary antibody (AF488) recognizing the anti-AQP4 antibody.[27, 57] Fluorescence intensity of NP linked to anti-AQP4 antibody was substantially higher than that of control NP preparations (Figure 1c).

Using TEM, the size and morphology of the polymer component of the various NP preparations was shown to be approximately constant for each of the NP preparations, regardless of the presence of MHA or resveratrol (Figures 1d-i). The fine structures within all of the NP preparations (Figure 1d-i) are magnetite nanoparticles encapsulated within the polymer sphere. Note that apparent aggregation was due to drying effects of sample preparation and the antibody component was not visible using TEM under the imaging conditions employed. The differences in contrast and visualization of the NP and the background carbon film spanning Cu grids observed in the images were due to subtle differences in instrument tuning and sample preparation: thinning of the edges of NP resulting in less material present for electrons to pass through and a resulting loss of contrast. Resveratrol loading in NP preparations was analyzed using HPLC and shown to be independent of polymer composition, ranging from 3.5 to 5.8 %

(mass of resveratrol/mass of dried NP). Release of resveratrol from NP was gradual, and close to completion following 3 hrs incubation in physiological solution at both pH 6 and 7 (Figures 1j-k). Note that resveratrol release was similar from each of the various NP preparations, regardless of antibody functionalisation; NP-MHA-Res are shown. The effects of a control preparation of free resveratrol was compared to an equivalent concentration of resveratrol encapsulated in NP. Resveratrol delivered by NP was at least as effective at reducing immunoreactivity of oxidative stress indicator carboxymethyl lysine, as an equivalent concentration of free resveratrol in an astrocyte-like immortalized Müller cell line (rMC1 cells, see Figure 1 in [58]).

Use of anti-AQP4 antibodies to target NP to astrocytes *in vitro*

We have previously demonstrated that AQP4 immunoreactivity increased in astrocytes of optic nerve vulnerable to secondary degeneration following partial injury *in vivo*.[34] Here, we provide further *in vitro* evidence that functionalizing NP with antibodies to AQP4 is a valid mechanism to direct NP to astrocytes following CNS injury. We demonstrate that immunoreactivity of AQP4 in astrocyte-like Müller cells within mixed retinal cultures increased following 48 hours and 7 days exposure to 10 mM glutamate (Figures 2a-b, a: 48 hours, * $P \leq 0.05$; b: 7 days, ** $P \leq 0.01$). AQP4 immunoreactivity was observed to colocalise with both GFAP+ Müller cells as well as βIII-tubulin+ retinal ganglion cells (Figures 2c-f) and was particularly pronounced in Müller cell end-feet following 7 days exposure to glutamate (white arrows; Figures 2d, f). Binding of the custom made antibody recognizing an extracellular epitope of AQP4 to GFAP+ rMC1 cells was confirmed immunohistochemically and shown to be distributed in punctate hotspots of florescence located at the cell membrane as well as in the cytosol (Figure 2g, h).

2′7′-dichlorofluorescein diacetate (DCFH-DA) conversion to DCF was used to monitor production of reactive species, as an indication of oxidative stress, in mixed retinal cells exposed to glutamate and treated with the various NP preparations. However, there were no significant differences in DCF fluorescence in cells treated with any of the NP preparations, including those containing resveratrol ($dF = 6$, $F = 1.722$, $P > 0.05$, Table 2), indicating lack of effective targeting and/ or delivery of therapeutic to cells within the mixed retinal cultures. Therefore, the interactions of NP preparations with mixed retinal cells were monitored using fluorescence immunohistochemistry *in vitro*, to directly assess the targeting efficiency of the anti-AQP4 antibody functionalized NP. It was observed that there was considerable clumping of NP and lack of targeting specificity of anti-AQP4 antibody functionalized NP to AQP4+ cells (Figure 3a, arrow indicating lack of targeting, arrowhead indicating clumping). There were no discernible consistent differences between the targeting and distribution behavior of the various NP preparations *in vitro*, regardless of the presence of resveratrol, MHA or anti-AQP4 antibody.

NP interactions are affected by biological milieu *in vitro*

Clumping and sedimentation of NP was not observed in NP stock suspended in Pluronic F-108. It was therefore hypothesized that elements of the tissue culture media were contributing to the lack of target specificity and clumping of the NP preparations.[59] *In vitro* incubation of NP with albumin, a key protein component of the fetal bovine serum used to supplement tissue culture media, resulted in a significant decrease in albumin concentration remaining in the supernatant after 24 hours incubation with each of the NP compositions, with the exception of NP with no functionalisation or resveratrol (Figure 3b, $dF = 7$, $F = 31.286$, $P \leq 0.05$). A decrease in the albumin concentration of the supernatant suggests the adsorption of albumin onto NP as a

corona.[60] The protein corona formed by serum proteins may interfere with the selective binding of anti-AQP4 antibody to cells and is likely to lead to the observed clumping of NP. Some of the possible interactions are illustrated in Figure 3c: note that the size, orientation and chemical linking of the protein corona to NP and/or antibody is speculative at this stage. Nevertheless, it is likely that *in vivo*, proteins including albumin, which is present in interstitial fluid,[61] could interact to form a corona surrounding the NP, binding through h-bonds, van der Waal interactions and solvation forces.[62]

It is interesting to note that the supernatant following incubation of albumin with NP-Res lacking MHA or antibody functionalisation *in vitro*, also displayed a reduced albumin concentration, indicating that MHA and/or antibody is not necessary for the NP-Albumin interaction (Figure 3b). Coating of NP-Res likely occurs *via* non-covalent interactions. Free resveratrol has been documented to bind to proteins found in cell media,[63] as well as albumin in aqueous solutions,[64] through spontaneous thermodynamically-favored processes.[65] Sequestering of resveratrol in an albumin-resveratrol complex may have contributed to our observed lack of effect of resveratrol containing NP on reactive species, following glutamate exposure *in vitro* (Table 2). Albumin-resveratrol complexes have been reported to exhibit a decreased absorbance band at 280 nm, the wavelength used to measure albumin concentration,[66] however in our hands we observed no decrease in absorbance of 6 mg/ml albumin at 280 nm in the presence of the 6 µg/ml concentration of resveratrol likely released from the NP (based on our measured mass of resveratrol/mass of dried NP and release profiles of Fig 1j, k), indicating lack of interference with our measures of albumin. Furthermore, we also assessed the amount of albumin bound directly to NP preparations with and without resveratrol and demonstrated a greater concentration of adsorbed albumin for NP-MHA-Res (1.89 ± 0.01 mg albumin/ mg NP) than

NP-MHA (1.17 ± 0.01 mg albumin/ mg NP). Taken together, the adsorption of albumin to NP regardless of the presence of antibody or resveratrol, confirms the presence of an albumin corona around each of the functionalized NP preparations. Thus, it can be concluded that multimodal polymeric functionalized NP containing antioxidants can be synthesized using the procedures employed. However, both their cell-specific targeting functionalisation and the effective delivery of their resveratrol therapeutic payload, may be modified by coating with serum proteins such as albumin *in vitro* and perhaps *in vivo*.

NP can be tracked *via* NanoSIMS, fluorescence microscopy and TEM *in vivo*

NanoSIMS is an imaging mass spectrometry technique, and has been used to track carbon compounds in biological systems using a ^{13}C isotope label.[67] Here we used ^{13}C–enriched resveratrol when synthesizing the NP in an attempt to track the release of Resveratrol *in vivo.* The presence of both Fe (Figure 4a-c) and ^{13}C (Figure 4d-f) in NP was confirmed by NanoSIMS analysis of bulk dried NP powder. The NP containing ^{13}C-enriched resveratrol were enriched to $2.14 \pm 5.21 \times 10^{-3}$ at% compared to empty NP ($0.98 \pm 3.13 \times 10^{-3}$ at%) and NP containing un-enriched resveratrol ($1.02 \pm 5.48 \times 10^{-3}$ at%; Figure 4d-f). A sample raw SIMS spectra (see Figure 2 in [58]) demonstrates that overlap of ^{56}Fe, $^{28}Si_2$ and $^{40}Ca^{16}O$ secondary ion signals at similar mass was only observed at 56.00 u. ^{56}Fe signal was successfully resolved for imaging, with spectral resolution shown in Table 1 in [58].

Equal concentrations of the various NP preparations were injected directly into the injury site following partial transection of the optic nerve in adult rats. Fe hotspots were present in NanoSIMS images of optic nerve from animals treated with NP, and are considered to correspond to magnetite encapsulated in NP (Figure 4g). These NanoSIMS images of Fe were

used to generate grey-scale bitmaps, which allowed delineation of the FOV into regions of Fe-hotspots (putative NP) and regions of non-Fe hotspots (Figure 4h). ROI for ^{13}C analysis were generated from these bitmaps, using set thresholds in Image-J analysis software (Figure 4i, Fe hotspots; j, non-Fe hotspot area).

Measurements of bracketing control samples gave a mean ratio of $1.10 \pm 5.29 \times 10^{-3}$ at%, indicating that the detection limit was about 0.01 at%. However, in all ROI for ^{13}C analysis, the $^{13}C/^{12}C$ ratio was within the error of the unlabeled control sample measurements, indicating that ^{13}C enrichment was less than the 0.01 at% detection limit. Furthermore, in optic nerve sections from animals injected at the injury site with NP containing ^{13}C–enriched Resveratrol (NP-MHA-Res, NP-MHA-Res-AB), C was uniformly distributed throughout the optic nerve tissue and there were no identifiable hotspots of ^{13}C signal apparent in any of the FOV imaged (Figure 5a). The observed lack of ^{13}C enrichment is likely due to the release and dissipation of ^{13}C-resveratrol from NP (Figure 1j, k) and its further dilution during sample preparation (using C-rich polymer resin, Lowacryl HM20). Modification of the polymer shell may slow down the release of resveratrol from NP and enable detection of ^{13}C-enriched therapeutic within the NP.[68, 69] Additionally, such a modification could be useful for therapeutic applications where more sustained release of antioxidant is desirable.

The localization of NP within treated optic nerve was tracked using NanoSIMS together with fluorescence microscopy. We have previously demonstrated that tissue types can be identified using NanoSIMS P, S and CN secondary ion maps collected in the form of RGB color maps, where the order of the secondary ion indicates the color channel in the RGB image. Differences in color indicate varying ratios of the secondary ions and correspond to different tissue types (e.g. glial vs axonal).[46] Darker blue regions in NanoSIMS false color P-S-CN RGB overlays

aligned with GFAP immunopositive regions (green) in sections adjacent to those used for NanoSIMS analysis (Figure 5b), as previously described,[46] allowing astrocyte rich glial tissue to be distinguished in NanoSIMS images. Note that glial regions may contain multiple cell types including astrocytes, oligodendrocyte somata, oligodendrocyte precursor cells, and inflammatory cells including macrophages. AQP4 immunoreactivity (yellow) was distributed predominantly in these glial regions (Figure 5c). NP were identified by detection of RhB (false colored red, Figure 5d) in the sections adjacent to those used for NanoSIMS analysis and by detection of hotspots of Fe signal in the NanoSIMS images. Note that NP are present in clusters within endocytic vesicles following *in vivo* administration to the injured optic nerve,[49] thereby facilitating visualization by fluorescence microscopy at the micron scale. Despite the 1 µm displacement between the adjacent tissue sections, RhB fluorescent NP occasionally aligned with hotspots of Fe signal (white, mass of 56 u; purple when aligned, Figure 5d) in the adjacent sections analyzed for NanoSIMS. Clusters of NP present in the tissue were likely to be smaller than the thickness of the tissue sections, and thus the NP detected using Fe signal in sections imaged using NanoSIMS only occasionally extended into adjacent sections, to also be detected by RhB fluorescence. RhB fluorescence (red) from NP-MHA-Res-AB was generally distributed close to AQP4 immunopositive (yellow) regions of optic nerve but was also present in AQP4 negative regions (Figure 5e), indicating a lack of exclusive targeting of the functionalized NP to AQP4, within astrocyte-rich glial regions *in vivo*. As expected, RhB fluorescence (red) and Fe hotspots (white) were only present above background in optic nerve from animals treated with the various NP preparations (Figures 5f-j), confirming that RhB fluorescence together with NanoSIMS provide a means of localizing NP within optic nerve sections. While Fe from ferritin could be visible in NanoSIMS images of injured optic nerves, we did not observe an increase in Fe hotspots as a

consequence of injury (Figure 5f compared to Figure 5g). NP-MHA-AB and NP-MHA-Res-AB were present predominantly in darker blue astrocyte-rich glial regions (Figure 5i, j), whereas NP-MHA-Res were distributed throughout the FOV (Figure 5h). It is possible that smaller clusters of NP, not able to be visualized by RhB fluorescence, may have been targeted more precisely to AQP4+ cells. However, there was also no indication of selective localization of Fe hotspots to astrocyte-rich glial regions in the NanoSIMS images from NP-MHA-Res treated animals (Figure 5h).

The localization of NP within treated optic nerves was assessed further using TEM and fluorescence immunohistochemistry. Spherical features encapsulating magnetite in a clearly circular distribution were visualized and identified as NP (some highlighted in red; Figures 5k-m). In optic nerve treated with anti-AQP4 functionalized NP containing resveratrol (NP-MHA-Res-AB), the NP were present extracellularly and in both astrocytes (Figure 5k), identified by characteristic filamentous features[70, 71] (arrow) and phagocytic cells likely to be macrophages (Figure 5l), identified by the abundance of glycogen granules in the soma,[72] suggesting that these NP can be internalized by both astrocytes and macrophages. Similar cellular localization was observed with NP-MHA-AB (not shown). In contrast, in optic nerve treated with NP containing resveratrol but not functionalized with anti-AQP4 antibody (NP-MHA-Res), NP were not observed in macrophages but were present extracellularly and within astrocytes (Figure 5m). Note also the proximity of the NP-containing cell to a myelinated axon at a Node of Ranvier (Figure 5m). These findings were confirmed by immunohistochemical analysis of optic nerve sections from treated animals: NP-MHA-Res-AB were present in and around ED1+ activated microglia/ macrophages (Figure 5n, arrow). In contrast, NP-MHA-Res were present in a more disperse distribution, occasionally in the proximity of ED1+ cells (arrow), but many not

associated with microglia/ macrophages (Figure 5o). Quantification of the proportion of ED1+ activated macrophages/microglia containing NP demonstrated that there was a significantly higher proportion of ED1+ cells that contained NP when animals were treated with NP-MHA-Res-AB than when they were treated with NP-MHA-Res ($P \leq 0.05$, Figure 5u). Thus, NP preparations can readily be tracked using NanoSIMS, fluorescence microscopy and TEM, and we have used these visualization and analysis techniques to demonstrate that while anti-AQP4 antibody functionalized NP were present in both astrocytes and macrophages, NP lacking the AQP4 antibody functionalisation generally evaded macrophages.

Functionalizing NP affects their localization and antioxidant efficacy *in vivo*

It has been reported that the presence of an albumin coating on polymer nanoparticles results in a significant decrease in uptake by macrophages.[73] The significant increase in nanoparticle size resulting from the formation of an corona of serum proteins is thought to decrease cellular uptake relative to corona-free nanoparticles.[74] However, it is important to note that when nanoparticles decorated with polyethylene glycol, designed to confer stealth-like properties to aid in macrophage evasion, are coated with serum proteins, phagocytosis by macrophages increases,[75] indicating that outcomes may depend upon the composition of the nanoparticles employed. Indeed, it is becoming increasingly understood that the accumulation of NP within cells, including macrophages, is highly dependent upon both the size and composition of the NP in question as well as the surrounding protein corona, and not solely dependent upon any single parameter.[76] Our *in vitro* demonstration of albumin binding to anti-AQP4 functionalized NP (Figure 3b) indicates that it is highly likely that these NP preparations are also coated by serum

proteins in the interstitial fluid *in vivo*, potentially interfering with targeting specificity. However, together with our further observation that NP-MHA-AB and NP-MHA-Res-AB are present at increased levels in macrophages *in vivo*, we conclude that the coating of NP with serum proteins including albumin, together with the anti-AQP4 antibody, appears to enhance macrophage phagocytosis of these polymeric NP. The increased immunogenicity introduced by attachment of the antibody to the NP may have contributed to their uptake by macrophages,[73, 77, 78] a phenomenon not necessarily restricted to use of anti-AQP4 antibodies. This interpretation is supported by the fact that NP lacking the anti-AQP4 antibody tended to evade macrophages. Alternatively, it is possible that the differences in conformation or orientation of the protein corona surrounding the various NP preparations affects interactions with macrophages (Figure 3c); and interactions may also depend upon the degree of activation or differentiation of the macrophages themselves.[79] Note that cell localization of NP functionalized with other antibodies could not be assessed in the current study due to the requirement for simultaneous processing for NanoSIMS analysis and the size of freeze-substitution systems. Additional *in vitro* and *in vivo* studies assessing the nature of the interactions between NP, antibodies, interstitial proteins and cells will be required to fully exploit the potential of multi-cellular targeting. Importantly, macrophage phagocytosis of NP could be beneficial if the therapeutic being delivered by the phagocytized NP can counter deleterious effects of macrophage infiltration.

We have recently demonstrated that reactive species in macrophages are increased at the injury site of a partial optic nerve transection 24 hours after injury, and are likely to initiate the spread of oxidative damage *via* the astrocytic syncytium.[32] Therefore, delivering an antioxidant to macrophages *via* the anti-AQP4 antibody functionalisation on NP could limit the effects of reactive species in macrophages and throughout the nerve. Indeed, the increased diffuse

immunoreactivity of 8-hydroxy-2'-deoxyguanosine (8OHdG), an indicator of oxidative damage to both mitochondrial and nuclear DNA,[80] observed in optic nerve sections following injury and PBS vehicle treatment relative to normal control (Figure 5p,q), was effectively decreased following treatment with NP-MHA-Res-AB (Figures 5t). NP-MHA-AB were less effective, with some non-nuclear 8OHdG immunoreactivity observed (Figure 5s), and NP-MHA-Res were ineffective (Figure 5r); note control image from section not incubated with anti-8OHdG antibody (Figure 5w). Semi-quantification of the area of 8OHdG immunointensity above an arbitrarily defined threshold intensity supported the observed decrease in tissue sections from animals treated with the NP-MHA-Res-AB (Figure 5v). The dispersed distribution of NP-MHA-Res through the optic nerve was further apparent (Figure 5r), with red, RhB containing NP present throughout the tissue section. It was not possible to confirm that 8OHdG immunoreactivity was decreased specifically in macrophages following NP-MHA-Res-AB treatment, as the wide emission spectrum of RhB present in NP in the sections precluded double label immunohistochemistry. Nevertheless, taken together our results indicate that delivery of resveratrol to macrophages was more effective at reducing oxidative damage across the nerve than diffuse release of resveratrol. As a further measure of cellular stress, we quantified the immunoreactivity of AQP4 in optic nerve sections from animals treated with the various NP preparations, demonstrating that AQP4 immunoreactivity following injury was only reduced when animals were treated with NP-MHA-Res-AB ($P \leq 0.05$, Figure 5x). These data provide an additional indication of the selective beneficial effects of delivery of antibody functionalized NP containing resveratrol to macrophages. Note that diffuse release of resveratrol can be implied from the rapid release of resveratrol from NP-MHA-Res observed *in vitro*, although additional effects of serum proteins such as albumin and/ or antibody sequestering resveratrol in or around

NP-MHA-Res-Ab cannot be ruled out. Additional control of oxidative stress in astrocytes by anti-AQP4 antibody functionalized NP containing resveratrol that evade macrophages and reach their intended target would likely provide further antioxidant benefit. However it is worth noting that NP-MHA-Res, which were observed in astrocytes, exerted no demonstrable beneficial effect on oxidative damage. A schematic diagram representing the observed cellular localizations of the various NP preparations *in vivo* is provided (Figure 6).

Effects of treatment with NP preparations on Ca microdomains *in vivo*

Further effects of the various NP preparations on changes in dynamics of Ca microdomains were assessed using NanoSIMS. Ca microdomains were observed in both glial and axonal regions of optic nerve, from animals in all treatment groups (Figure 7a-e). Note that glial and axonal regions were identified with reference to P-S-CN false color RGB NanoSIMS images, together with immunohistochemical analysis of adjacent sections, as described above[46]. Sequential imaging of the same FOV revealed changes to microdomains along the z-plane, allowing three-dimensional imaging of Ca microdomains using NanoSIMS (see Figure 3 in [58]). Some Ca microdomains were co-located with areas of enriched P signal, as reported previously.[46] However, analysis of microdomains was confined to the density and proportion of microdomains that were not co-located with areas of enriched P signal (non-P co-localized) in glial and axonal regions, as these are the outcomes that we have demonstrated to decrease following partial optic nerve transection *in vivo*.[46] In the current study, there was a strong trend towards reduced density and proportion of Ca microdomains in optic nerve vulnerable to secondary degeneration following partial optic nerve transection. However, all changes relative to normal or vehicle treated injured optic nerve were not statistically significant for either axonal, glial or pooled

tissue compartments (Figure 7f-i $P > 0.05$). Reduced density of Ca microdomains may reflect release of Ca^{2+} into the cytosol, resulting in increased reactive species and oxidative stress.[46] Interestingly, there was a statistically significant increase in both density and proportion of Ca microdomains in glial regions, compared to axonal regions, in optic nerve from animals treated with NP-MHA-Res (Figure 7f, g $P \leq 0.05$). This aberrant change was associated with continued increased 8OHdG and AQP4 immunoreactivity, indicating continued oxidative and cellular stress (Figure 5r, v, x). In contrast, an increasing trend towards normalization of Ca microdomains in axonal tissue compartments, which was only apparent following treatment of animals with anti-AQP4 antibody functionalized NP containing resveratrol (NP-Res-MHA-Ab) (Figures 7f, g), correlated with reduced oxidative damage to DNA and reduced AQP4 immunoreactivity (Figure 5t, v, x). The variability of the Ca microdomain data derived from NanoSIMS is a feature of these analyses and reflects the relatively small area of the nerve that it is possible to sample, relative to the whole tissue section.[46]

NP preparations affect functional outcomes

While differential effects were demonstrated using a series of oxidative stress outcome measures (Figure 5), of particular importance given the inclusion of the anti-oxidant resveratrol, further indices of improvement were considered. We have previously demonstrated that neuronal retinal ganglion cells vulnerable to secondary degeneration die *via* both apoptotic and necrotic mechanisms following partial optic nerve transection[81]. However we have also learnt that death of retinal ganglion cells does not always directly reflect the all-important functional outcomes[82]. We therefore focused on behavioural measures of visual function as the most relevant measure to assess therapeutic efficacy of the NP system. The optokinetic nystagmus visual reflex was used

as a measure of visual function retained by the injured optic nerve, relative to that of the right optic nerve of normal uninjured animals. As expected, a significant decrease was observed in mean total responses following injury in untreated animals (PBS vehicle) compared to uninjured normal animals (Figure 7j, $P \leq 0.05$).[53] Treatment with NP-MHA-Res resulted in no improvement in the number of responses: values remained significantly lower than for normal animals ($P \leq 0.05$). Treatment with anti-AQP4 antibody targeted NP, both non-resveratrol containing (NP-MHA-AB) and resveratrol containing (NP-MHA-Res-AB), resulted in numbers of responses that were not significantly different to normal animals ($P > 0.05$). However, only treatment with NP-MHA-Res-AB resulted in a significant increase in the number of responses compared to PBS vehicle treated control animals ($P \leq 0.05$). Functional outcomes mirror the 8OHdG and AQP4 immunoreactivity observed in optic nerve sections (Figures 5p-t), indicating a link between oxidative damage in the optic nerve and functional outcomes at 24 hours post injury. As such, we demonstrate a functionally significant therapeutic effect from the application of anti-AQP4 antibody functionalized resveratrol containing NP 24 hours following injury.

CONCLUSIONS

In summary, we have developed an antibody-functionalized polymer NP, which interacts with endogenous interstitial proteins such as albumin to form a highly effective therapeutic strategy for treatment of secondary degeneration *in vivo*. Antibody functionalisation resulted in NP entering macrophages and delivering the antioxidant resveratrol where it was most beneficial. Treatment with NP-MHA-Res-AB resulted in behavioral outcomes comparable to uninjured animals, associated with reduced oxidative damage to DNA, reduced AQP4 immunointensity and a trend towards normal Ca microdomain distributions in axons. Each NP preparation was

present extracellularly and within astrocytes, regardless of anti-AQP4 antibody functionalisation. However, diffuse delivery of resveratrol by non-functionalized NP, without the additional macrophage targeting provided by antibody functionalisation, was ineffective at preserving function. This suggests that the delivery of the antioxidant resveratrol to macrophages, perhaps in conjunction with delivery to astrocytes, plays a crucial role in mitigating the effects of secondary degeneration in the optic nerve following injury. Preventing or delaying the spread of reactive species by macrophages together with protection of astrocytes may leave astrocytes free to preserve axons and thus function in the CNS. We demonstrate the potential benefits from successful development of multimodal, targeted NP for the treatment of CNS injury, and highlight the need for comprehensive investigation of NP location, interactions and effects, both *in vitro* and *in vivo*, in order to work towards full understanding of functional outcomes.

ACKNOWLEDGEMENTS

This work was supported by the National Health and Medical Research Council of Australia (Grant ID: APP1028681 and APP1082403). We thank Associate Professor Gabriel A. Silva at the Shiley Eye Center at the University of San Diego, CA, for gifting us a sample of rMC1 retinal Müller cells; Igor Luzinov, University of North Carolina for donating PGMA; Mr Guy Ben-Ary of Cell Central, The University of Western Australia, for assistance with fluorescence microscopy; Mr John Murphy, The University of Western Australia, for assistance with confocal microscopy; Professor Martin Saunders for assistance with TEM, Dr Paul Guagliardo and Assistant Professor Jeremy Bougoure for assistance with NanoSIMS. The authors acknowledge the facilities, scientific and technical assistance of the Australian Microscopy and Microanalysis Research Facility at the Centre for Microscopy, Characterisation and Analysis, The University of Western Australia, a facility funded by the University, State and Commonwealth Governments.

This work was made possible in part by the OpenMIMS software whose development is funded by the NIH/NIBIB National Resource for Imaging Mass Spectrometry, NIH/NIBIB 5P41 EB001974-10.

TABLES

Table 1: DLS size and zeta potential measurements of NP preparations

NP Composition	Size (nm)	Zeta Potential
NP-e	168.8 ± 30.5	-11.6 ± 12.1
NP-MHA	148.2 ± 20.9	-19.9 ± 5.1
NP-MHA-AB	330.5 ± 32.6	-20.4 ± 8.4
NP-Res	115.4 ± 18.9	-30.3 ± 4.5
NP-MHA-Res	125.5 ± 18.8	-30.4 ± 5.2
NP-MHA-Res-AB	214.3 ± 44.1	-18.4 ± 10.9

The presence of MHA or resveratrol did not influence the overall NP diameter measured using DLS. Functionalisation of NP with anti-AQP4 antibody resulted in an observable increase in size, but did not influence the zeta potential.

Table 2: Effect of various NP preparations on DCF fluorescence intensity in mixed retinal cells stressed with glutamate

NP Composition	Mean DCF fluorescence intensity/mg protein (± S.E.M.)
Control	5.94 ± 1.74
NP-e	4.94 ± 0.89
NP-MHA	3.91 ± 0.40
NP-Res	3.91 ± 0.29
NP-MHA-Res	6.71 ± 1.14
NP-MHA-AB	7.55 ± 1.22
NP-MHA-Res-AB	4.91 ± 1.03

Mean DCF fluorescence intensity (arbitrary units) in mixed retinal cells stressed with 10 mM glutamate and treated with various NP preparations for 24 hours or

vehicle only control: no significant differences were observed.

FIGURE LEGENDS

FIGURE 1: Synthesis and characterization of NP preparations. (a) A maleimide functional group was attached to the polymer chain, resulting in the formation of an ester linkage through a ring opening reaction of the epoxide ring on the PGMA backbone and the carboxylic acid on the 6-maleimidohexanoic acid.[56] *(b) The maleimide functional group facilitates attachment of anti-AQP4 antibody (green). (c) Confirmation of attachment of anti-AQP4 antibody to NP is shown via increased green fluorescence following incubation of NP-MHA-AB with species specific AF488 secondary antibody (NP + 1˚ + 2˚), compared to NP-MHA with AF488 secondary antibody (NP + 2˚), NP-MHA-AB but no secondary antibody control (NP + 1˚), or NP incubated with no antibodies (NP); data are mean fluorescence ± S.E.M. (d-i) NP preparations were visualized using TEM (d, NP-e; e, NP-MHA; f, NP-MHA-AB; g, NP-Res; h, NP-MHA-Res; i, NP-MHA-Res-AB; AB = anti-AQP4 antibody, Res = resveratrol), scale bar = 200 nm. HPLC was used to analyze resveratrol release from NP (NP-MHA-Res) over 360 minutes in PBS at (j) pH 6 (k) pH 7 (mean ± S.E.M.), both as the percentage of resveratrol in each analyzed sample (solid line with upright triangle) and the cumulative resveratrol (spread dotted line with inverted triangle) as a percentage of resveratrol present in the initial sample. The line above 0 (dashed line) indicates the resveratrol content in NP at the termination of the experiment (360 minutes) and the line at approximately 80% (tight dotted line) indicates the total resveratrol measured at 360 minutes (cumulative resveratrol in reservoir/sink plus remaining resveratrol in NP). Resveratrol release data presented are representative of two independent experiments.*

FIGURE 2: Increase in AQP4 immunoreactivity in mixed retinal cells exposed to glutamate for 48 hours or 7 days in vitro. Glutamate (10 mM) exposure resulted in a significant increase in

*mean AQP4 immunofluorescence co-localized with GFAP+ astrocytic like Müller cells at (a) 48 hr and (b) 7 days (*P ≤ 0.05, **P ≤ 0.01; mean ± S.E.M.). (c, d) Representative images show increased AQP4 immunoreactivity following 7 days glutamate exposure, (e, f) in both Müller cells and retinal ganglion cells: red = AQP4, green = GFAP, purple = βIII Tubulin, blue = Hoechst+ nuclei. White arrows indicate co-localization, scale bar = 50 µm. (g-h) Immunoreactivity of custom made anti-AQP4 antibody in a single 0.5 µm optical slice in the z plane of rMC-1 cells in vitro (g, secondary only control; h, anti-AQP4 antibody, green (serum 1A6); scale bar = 20 µm). Data are representative of at least three independent experiments.*

*FIGURE 3: Behavior of NP preparations in vitro. (a) Representative image (individual 0.5 µm optical slice in the z-plane) of mixed retinal cells incubated with nanoparticles (NP-MHA-AB; Blue = Hoechst, Green = AQP4 and Red = Nanoparticles (RhB); scale bar = 30 µm, arrowhead indicates clump of NP, arrow indicates NP not associated with AQP4+ cell). (b) Histogram shows concentration of albumin in the supernatant after 24 hours of incubation with suspended NP of varying composition (mean albumin concentration ± S.E.M., * P < 0.05 compared to Albumin 0 hrs, † P < 0.05 compared to Albumin 24 hrs and ‡ P < 0.05 compared to empty NP). (c) Schematic diagram illustrating potential interactions of the protein corona (yellow ovals) including albumin, likely to form around NP following their incubation in biological media. The size and orientation of the protein corona relative to antibody and/ or resveratrol is speculative at this stage. Data are representative of two independent experiments.*

FIGURE 4: Analysis of ^{13}C content and Fe distribution in NP and following injection of NP into injured optic nerve in vivo. (a-c) NanoSIMS analysis of dried NP mounted directly onto a Si

wafer substrate shows clear Fe signal at 56 u for NP that are (a) not loaded with resveratrol, (b) loaded with un-enriched resveratrol or (c) loaded with ^{13}C-enriched resveratrol. Similarly, (d-f) HSI images of the $^{13}C^{12}C/^{12}C^{12}C$ ratio showing the relative ^{13}C content in NP that are (d) not loaded with resveratrol, (e) loaded with un-enriched resveratrol, (f) loaded with ^{13}C-enriched resveratrol; scale bar = 10 μm; scale from blue to pink indicates enrichment in ^{13}C, (blue = natural abundance). (g) Fe hotspots in NanoSIMS images of optic nerve tissue were used to generate (h) greyscale bitmaps indicating ROI type (RGB code; Fe-hotspots = 141414, remaining tissue = 323232 and holes in tissue = b3b3b3). (i) Bitmaps were used to generate ROIs for Fe hotspots and (j) for remaining tissue, that were used to extract signal intensity data from $^{13}C^{12}C^{-}$ images, scale bar = 10 μm. Data are representative of multiple sections from n=4 animals per group, collected in a single large scale experiment.

FIGURE 5: NanoSIMS, fluorescence and TEM imaging of optic nerve tissue following partial optic nerve transection injury and treatment with various NP preparations. Note that all images are from animals that have received the partial optic nerve transection injury unless designated 'normal'. (a) ^{13}C, detected as $^{13}C^{12}C^{-}$ secondary ion (25 u), was evenly distributed throughout the FOV. (b) Astrocyte-rich glial areas in NanoSIMS images were identified by superimposing GFAP immunoreactivity (green fluorescence) on P-S-CN false-color RGB overlays. (c) AQP4 immunoreactivity (yellow fluorescence) was superimposed on P-S-CN images to demonstrate that AQP4 was localized predominantly in astrocyte-rich glial regions. (d) Superimposing RhB fluorescence (red) on NanoSIMS Fe images demonstrated occasional co-localization of RhB with Fe hotspots (white, purple when co-localized). (e) Fluorescence images demonstrated that anti-AQP4 antibody functionalized NP (NP-MHA-Res-AB, RhB fluorescence signal, red) did not

specifically associate with AQP4 immunoreactivity (yellow). (f-j) Fluorescence images superimposed on P-S-CN NanoSIMS images demonstrated that Fe hotspots (white) and RhB (red) fluorescence were not above background in optic nerve from Normal (f) or PBS-vehicle (g) treated animals, but were seen following (h) NP-MHA-Res, (i) NP-MHA-AB and (j) NP-MHA-Res-AB treatment, although not specifically localized to glial regions. (k-m) TEM micrographs show the presence of NP within optic nerve: the spherical polymer NPs (some highlighted in red to aid visualization) contain smaller Fe_3O_4 nanoparticles (black). NP-MHA-Res-AB were found within (k) astrocytes and (l) macrophages, scale bar = 400 nm, whereas NP-MHA-Res were confined to astrocytes (m), scale bar = 1 µm, arrows indicates astrocytic filament-like structures. (n-o) Fluorescence immunohistochemistry demonstrated (n) NP-MHA-Res-AB (pink) clustered in and around ED1+ (green) macrophages (arrow) whereas (o) NP-MHA-Res were distributed diffusely across the section, scale bars = 10 µm. (p-t) Fluorescence immunohistochemistry demonstrated increased diffuse 8OHdG immunoreactivity (green) in (q) injured PBS-vehicle treated animals compared to (p) normal: (r) NP-MHA-Res had no effect, (s) NP-MHA-AB partially reduced 8OHdG and (t) NP-MHA-Res-AB comprehensively reduced non- nuclear 8OHdG immunoreactivity (blue = Hoechst, red = RhB from NP, scale bar = 40 µm). (u) Quantification of the mean ± SEM proportion of ED1+ activated microglia/ macrophages containing NP; (v) quantification of mean ± SEM area of 8OHdG immunoreactivity above an arbitrarily defined threshold intensity; (w) control NP-MHA-AB image demonstrating appearance of section following immunohistochemistry where the primary antibody was omitted, scale bar = 40 µm; (x) quantification of mean ± SEM AQP4 immunointensity above an arbitrarily defined threshold intensity. Data are representative of multiple sections from n=4

*animals per group, collected in a single large scale experiment; * indicates significant difference $P \leq 0.05$.*

FIGURE 6: (1) Nanoparticles enter the biological milieu in vivo and (2) interact with endogenous proteins resulting in the formation of a protein corona around the particles. Three nanoparticle formulations were tested in vivo which were shown to interact with albumin in vitro; (a) NP-MHA-Res-AB, (b) NP-MHA-AB and (c) NP-MHA-Res. (3) The presence of a corona composed of endogenous proteins allows some nanoparticles to evade macrophages. (4) Some antibody conjugated nanoparticles are phagocytized by macrophages. (5) All three nanoparticle compositions are internalized by astrocytes.

FIGURE 7 (a-e) Representative NanoSIMS images of Ca superimposed on P-S-CN show Ca microdomains (red) in (a) Normal uninjured optic nerve, and following partial optic nerve transection and treatment with (b) PBS vehicle, (c) NP-MHA-Res, (d) NP-MHA-AB and (e) NP-MHA-Res-AB, scale bar = 10 μm. Dot plots show quantification of both axonal and glial mean ± S.E.M. non-P co-localized Ca microdomain (f) density (number per mm^2) and (g) proportion (mm^2 of microdomain per mm^2 of tissue area) in optic nerve from normal uninjured animals and from optic nerve vulnerable to secondary degeneration following partial optic nerve transection and treatment with PBS vehicle, or the various NP preparations. Significant differences between axonal (blue) and glial (red) values are indicated ($P \leq 0.05$). Data obtained from pooling axonal and glial values is also shown for (h) density and (i) proportion. Circles indicate mean for each animal within a given treatment group, vertical bars illustrate the range and horizontal bars indicate grand means for each treatment group. Data points at the same value are shown as*

two circles (one larger). (j) Histogram shows mean ± S.E.M. total responses in the optokinetic nystagmus reflex test of visual behavior by PVG rats, assessing normal uninjured animals or 24 hours following partial optic nerve transection and administration of PBS vehicle control or NP preparations. Significant differences are indicated relative to treatment with NP-MHA-Res-AB ($P \leq 0.05$) or to completely normal uninjured animals (‡ $P \leq 0.05$). Data are representative of multiple sections (where appropriate) from n=4 animals per group, collected in a single large scale experiment.*

ABBREVIATIONS

AQP4, Aquaporin 4; BSA, Bovine serum albumin; CNS, Central nervous system; DCF, Dichlorofluorescein; DCFH-DA, 2',7'-Dichlorodihydrofluorescein diacetate; DLS, Dynamic light scattering; DMEM, Dulbecco's modified Eagle's medium; DNA, Deoxyribonucleic acid; FOV, Field of view; GFAP, Glial fibrillary acidic protein; HPLC, High-performance liquid chromatography; MEK, Methyl ethyl ketone; MHA, 6-Maleimidohexanoic acid ; NanoSIMS, Nanoscale secondary ion mass-spectrometry; NMR, Nuclear magnetic resonance; NP-e, PGMA-RhB nanosphere with no resveratrol; NP-MHA, PGMA-MHA-RhB nanosphere with no resveratrol; NP-MHA-AB, PGMA-RhB nanosphere with conjugated anti-AQP4 antibody and no resveratrol ; NP-MHA-Res, PGMA-MHA-RhB nanosphere encapsulating resveratrol; NP-MHA-Res-AB, PGMA-RhB nanosphere with conjugated anti-AQP4 antibody encapsulating resveratrol; NP-Res, PGMA-RhB nanosphere encapsulating resveratrol; NP-Res, PGMA-RhB nanosphere encapsulating resveratrol; NPs , Polymer nanoparticles; PBS, Phosphate buffered saline; PGMA, Poly(glycidyl methacrylate); PVG, Piebald Viral Glaxo (rats); RCF, Relative centrifugal force ; RhB, Rhodamine B; rMC-1 , Retinal Müller glial cell-line 1; ROI, Region of interest; TCEP, *tris*(2-carboxyethyl)phosphine; TEM, Transmission electron microscopy.

REFERENCES

1. Hamilton, N.; Vayro, S.; Kirchhoff, F.; Verkhratsky, A.; Robbins, J.; Gorecki, D. C.Butt, A. M. Mechanisms of Atp- and Glutamate-Mediated Calcium Signaling in White Matter Astrocytes. *Glia* **2008**, 56, 734-749
2. Li, S.Stys, P. K. Mechanisms of Ionotropic Glutamate Receptor-Mediated Excitotoxicity in Isolated Spinal Cord White Matter. *The Journal of Neuroscience* **2000**, 20, 1190-1198
3. Davidson, S. M.Duchen, M. R. Calcium Microdomains and Oxidative Stress. *Cell Calcium* **2006**, 40, 561-574
4. Peng, T.-I.Jou, M.-J. Oxidative Stress Caused by Mitochondrial Calcium Overload. *Annals of the New York Academy of Sciences* **2010**, 1201, 183-188
5. Fitzgerald, M.; Bartlett, C. A.; Harvey, A. R.Dunlop, S. A. Early Events of Secondary Degeneration after Partial Optic Nerve Transection: An Immunohistochemical Study. *Journal of Neurotrauma* **2010**, 27, 439-452
6. Payne, S. C.; Bartlett, C. A.; Harvey, A. R.; Dunlop, S. A.Fitzgerald, M. Chronic Swelling and Abnormal Myelination During Secondary Degeneration after Partial Injury to a Central Nervous System Tract. *Journal of Neurotrauma* **2011**, 28, 1077-1088
7. Payne, S. C.; Bartlett, C. A.; Harvey, A. R.; Dunlop, S. A.Fitzgerald, M. Myelin Sheath Decompaction, Axon Swelling, and Functional Loss During Chronic Secondary Degeneration in Rat Optic Nerve. *Investigative Ophthalmology & Visual Science* **2012**, 53, 6093-6101
8. Puttfarcken, P. S.; Getz, R. L.Coyle, J. T. Kainic Acid-Induced Lipid Peroxidation: Protection with Butylated Hydroxytoluene and U78517f in Primary Cultures of Cerebellar Granule Cells. *Brain Research* **1993**, 624, 223-232
9. Slemmer, J. E.; Shacka, J. J.; Sweeney, M. I.Weber, J. T. Antioxidants and Free Radical Scavengers for the Treatment of Stroke, Traumatic Brain Injury and Aging. *Current Medicinal Chemistry* **2008**, 15, 404-414
10. Grotta, J.; Clark, W.; Coull, B.; Pettigrew, L. C.; Mackay, B.; Goldstein, L. B.; Meissner, I.; Murphy, D.LaRue, L. Safety and Tolerability of the Glutamate Antagonist Cgs 19755 (Selfotel) in Patients with Acute Ischemic Stroke: Results of a Phase Iia Randomized Trial. *Stroke* **1995**, 26, 602-605
11. Kohara, A.; Okada, M.; Tsutsumi, R. I. E.; Ohno, K.; Takahashi, M.; Shimizu-Sasamata, M.; Shishikura, J.-I.; Inami, H.; Sakamoto, S.Yamaguchi, T. In-Vitro Characterization of Ym872, a Selective, Potent and Highly Water-Soluble A-Amino-3-Hydroxy-5-Methylisoxazole-4-Propionate Receptor Antagonist. *Journal of Pharmacy and Pharmacology* **1998**, 50, 795-801
12. de Almeida, L. M. V.; Leite, M. C.; Thomazi, A. P.; Battu, C.; Nardin, P.; Tortorelli, L. S.; Zanotto, C.; Posser, T.; Wofchuk, S. T.; Leal, R. B.*, et al.* Resveratrol Protects against Oxidative Injury Induced by H2o2 in Acute Hippocampal Slice Preparations from Wistar Rats. *Archives of Biochemistry and Biophysics* **2008**, 480, 27-32
13. Hsieh, T.-c.; Lu, X.; Wang, Z.Wu, J. M. Induction of Quinone Reductase Nqo1 by Resveratrol in Human K562 Cells Involves the Antioxidant Response Element Are and Is Accompanied by Nuclear Translocation of Transcription Factor Nrf2. *Medicinal Chemistry* **2006**, 2, 275-285
14. Tsai, S.-K.; Hung, L.-M.; Fu, Y.-T.; Cheng, H.; Nien, M.-W.; Liu, H.-Y.; Zhang, F. B.-Y.Huang, S.-S. Resveratrol Neuroprotective Effects During Focal Cerebral Ischemia Injury Via Nitric Oxide Mechanism in Rats. *Journal of Vascular Surgery* **2007**, 46, 346-353

15. Lin, C. J.; Chen, T. H.; Yang, L. Y.Shih, C. M. Resveratrol Protects Astrocytes against Traumatic Brain Injury through Inhibiting Apoptotic and Autophagic Cell Death. *Cell Death and Disease* **2014**, 5, e1147
16. Shin, J. Y.; Seo, M. A.; Choi, E. J.; Kim, J. K.; Seo, E. S.; Lee, J. H.; Chung, H. L.Kim, W. T. Neuroprotective Effects of Resveratrol Via Anti-Apoptosis on Hypoxic-Ischemic Brain Injury in Neonatal Rats. *Korean Journal of Pediatrics* **2008**, 51, 1102-1111
17. Sönmez, Ü.; Sönmez, A.; Erbil, G.; Tekmen, I.Baykara, B. Neuroprotective Effects of Resveratrol against Traumatic Brain Injury in Immature Rats. *Neuroscience Letters* **2007**, 420, 133-137
18. Goldberg, D. M.; Yan, J.Soleas, G. J. Absorption of Three Wine-Related Polyphenols in Three Different Matrices by Healthy Subjects. *Clinical Biochemistry* **2003**, 36, 79-87
19. Walle, T.; Hsieh, F.; DeLegge, M. H.; Oatis, J. E.Walle, U. K. High Absorption but Very Low Bioavailability of Oral Resveratrol in Humans. *Drug Metabolism and Disposition* **2004**, 32, 1377-1382
20. Morris, G. F.; Bullock, R.; Marshall, S. B.; Marmarou, A.; Maas, A.Marshall, L. F. Failure of the Competitive N-Methyl-D-Aspartate Antagonist Selfotel (Cgs 19755) in the Treatment of Severe Head Injury: Results of Two Phase Iii Clinical Trials. *Journal of Neurosurgery* **1999**, 91, 737-743
21. Labiche, L.Grotta, J. Clinical Trials for Cytoprotection in Stroke. *Neurotherapeutics: The Journal of the American Society for Experimental NeuroTherapeutics* **2004**, 1, 46-70
22. Asensi, M.; Medina, I.; Ortega, A.; Carretero, J.; Baño, M. C.; Obrador, E.Estrela, J. M. Inhibition of Cancer Growth by Resveratrol Is Related to Its Low Bioavailability. *Free Radical Biology & Medicine* **2002**, 33, 387-398
23. Anand, P.; Kunnumakkara, A. B.; Newman, R. A.Aggarwal, B. B. Bioavailability of Curcumin: Problems and Promises. *Molecular Pharmaceutics* **2007**, 4, 807-818
24. Ikonomidou, C.Turski, L. Why Did Nmda Receptor Antagonists Fail Clinical Trials for Stroke and Traumatic Brain Injury? *The Lancet Neurology* **2002**, 1, 383-386
25. Evans, C. W.; Latter, M. J.; Ho, D.; Peerzade, S. A. M. A.; Clemons, T. D.; Fitzgerald, M.; Dunlop, S. A.Iyer, K. S. Multimodal and Multifunctional Stealth Block Copolymer Nanospheres for Sustained Drug Delivery. *New Journal of Chemistry* **2012**, 36, 1457-1462
26. Xie, J.; Lee, S.Chen, X. Nanoparticle-Based Theranostic Agents. *Advanced Drug Delivery Reviews* **2010**, 62, 1064-1079
27. Johnston, A. P. R.; Kamphuis, M. M. J.; Such, G. K.; Scott, A. M.; Nice, E. C.; Heath, J. K.Caruso, F. Targeting Cancer Cells: Controlling the Binding and Internalization of Antibody-Functionalized Capsules. *ACS Nano* **2012**, 6, 6667-6674
28. Sarfati, G.; Dvir, T.; Elkabets, M.; Apte, R. N.Cohen, S. Targeting of Polymeric Nanoparticles to Lung Metastases by Surface-Attachment of Yigsr Peptide from Laminin. *Biomaterials* **2011**, 32, 152-161
29. Ashley, C. E.; Carnes, E. C.; Phillips, G. K.; Padilla, D.; Durfee, P. N.; Brown, P. A.; Hanna, T. N.; Liu, J.; Phillips, B.; Carter, M. B.*, et al.* The Targeted Delivery of Multicomponent Cargos to Cancer Cells by Nanoporous Particle-Supported Lipid Bilayers. *Nature Materials* **2011**, 10, 389-397
30. Silva, G. A. Nanotechnology Applications and Approaches for Neuroregeneration and Drug Delivery to the Central Nervous System. *Annals of the New York Academy of Sciences* **2010**, 1199, 221-230

31. Lobsiger, C. S.Cleveland, D. W. Glial Cells as Intrinsic Components of Non-Cell-Autonomous Neurodegenerative Disease. *Nature Neuroscience* **2007**, 10, 1355-1360
32. O'Hare Doig, R. L.; Bartlett, C. A.; Maghzal, G. J.; Lam, M.; Archer, M.; Stocker, R.Fitzgerald, M. Reactive Species and Oxidative Stress in Optic Nerve Vulnerable to Secondary Degeneration. *Experimental Neurology* **2014**, 261, 136-146
33. Gunnarson, E.; Zelenina, M.Aperia, A. Regulation of Brain Aquaporins. *Neuroscience* **2004**, 129, 945-953
34. Wells, J.; Kilburn, M. R.; Shaw, J. A.; Bartlett, C. A.; Harvey, A. R.; Dunlop, S. A.Fitzgerald, M. Early in Vivo Changes in Calcium Ions, Oxidative Stress Markers, and Ion Channel Immunoreactivity Following Partial Injury to the Optic Nerve. *Journal of Neuroscience Research* **2012**, 90, 606-618
35. Meloni, B. P.; Milani, D.; Edwards, A. B.; Anderton, R. S.; O'Hare Doig, R. L.; Fitzgerald, M.; Palmer, T. N.Knuckey, N. W. Neuroprotective Peptides Fused to Arginine-Rich Cell Penetrating Peptides: Neuroprotective Mechanism Likely Mediated by Peptide Endocytic Properties. *Pharmacol Ther* **2015**, 153, 36-54
36. Bendszus, M.Stoll, G. Caught in the Act: In Vivo Mapping of Macrophage Infiltration in Nerve Injury by Magnetic Resonance Imaging. *The Journal of Neuroscience* **2003**, 23, 10892-10896
37. Fitzgerald, M.; Bartlett, C. A.; Evill, L.; Rodger, J.; Harvey, A. R.Dunlop, S. A. Secondary Degeneration of the Optic Nerve Following Partial Transection: The Benefits of Lomerizine. *Experimental Neurology* **2009**, 216, 219-230
38. Block, M. L.; Zecca, L.Hong, J.-S. Microglia-Mediated Neurotoxicity: Uncovering the Molecular Mechanisms. *Nature Reviews Neuroscience* **2007**, 8, 57-69
39. Fleming, J. C.; Norenberg, M. D.; Ramsay, D. A.; Dekaban, G. A.; Marcillo, A. E.; Saenz, A. D.; Pasquale-Styles, M.; Dietrich, W. D.Weaver, L. C. The Cellular Inflammatory Response in Human Spinal Cords after Injury. *Brain* **2006**, 129, 3249-3269
40. Harrison, J.; Bartlett, C. A.; Cowin, G.; Nicholls, P. K.; Evans, C. W.; Clemons, T. D.; Zdyrko, B.; Luzinov, I. A.; Harvey, A. R.; Iyer, K. S.*, et al.* In Vivo Imaging and Biodistribution of Multimodal Polymeric Nanoparticles Delivered to the Optic Nerve. *Small* **2012**, 8, 1579-1589
41. Labarre, P.; Papon, J.; Rose, A. H.; Guerquin-Kern, J.-L.; Morandeau, L.; Wu, T.-d.; Moreau, M.-F.; Bayle, M.; Chezal, J.-M.; Croisy, A.*, et al.* Melanoma Affinity in Mice and Immunosuppressed Sheep of [125i]N-(4-Dipropylaminobutyl)-4-Iodobenzamide, a New Targeting Agent. *Nuclear Medicine and Biology* **2008**, 35, 783-791
42. Bonnet-Duquennoy, M.; Papon, J.; Mishellany, F.; Labarre, P.; Guerquin-Kern, J.-L.; Wu, T.-D.; Gardette, M.; Maublant, J.; Penault-Llorca, F.; Miot-Noirault, E.*, et al.* Targeted Radionuclide Therapy of Melanoma: Anti-Tumoural Efficacy Studies of a New 131i Labelled Potential Agent. *International Journal of Cancer* **2009**, 125, 708-716
43. Gardette, M.; Papon, J.; Bonnet, M.; Desbois, N.; Labarre, P.; Wu, T.-D.; Miot-Noirault, E.; Madelmont, J.-C.; Guerquin-Kern, J.-L.; Chezal, J.-M.*, et al.* Evaluation of New Iodinated Acridine Derivatives for Targeted Radionuclide Therapy of Melanoma Using 125i, an Auger Electron Emitter. *Investigational New Drugs* **2011**, 29, 1253-1263
44. Peixoto, P.; Zeghida, W.; Carrez, D.; Wu, T.-D.; Wattez, N.; Croisy, A.; Demeunynck, M.; Guerquin-Kern, J.-L.Lansiaux, A. Unusual Cellular Uptake of Cytotoxic 4-Hydroxymethyl-3-Aminoacridine. *European Journal of Medicinal Chemistry* **2009**, 44, 4758-4763
45. Legin, A. A.; Schintlmeister, A.; Jakupec, M. A.; Galanski, M.; Lichtscheidl, I.; Wagner, M.Keppler, B. K. Nanosims Combined with Fluorescence Microscopy as a Tool for Subcellular

Imaging of Isotopically Labeled Platinum-Based Anticancer Drugs. *Chemical Science* **2014**, 5, 3135-3143
46. Lozić, I.; Bartlett, C. A.; Shaw, J. A.; Iyer, K. S.; Dunlop, S. A.; Kilburn, M. R.Fitzgerald, M. Changes in Subtypes of Ca Microdomains Following Partial Injury to the Central Nervous System. *Metallomics* **2014**, 6, 455-464
47. Kopp, C.; Wisztorski, M.; Revel, J.; Mehiri, M.; Dani, V.; Capron, L.; Carette, D.; Fournier, I.; Massi, L.; Mouajjah, D.*, et al.* Maldi-Ms and Nanosims Imaging Techniques to Study Cnidarian–Dinoflagellate Symbioses. *Zoology* **2014**,
48. Sun, S.; Zeng, H.; Robinson, D. B.; Raoux, S.; Rice, P. M.; Wang, S. X.Li, G. Monodisperse Mfe2o4 (M = Fe, Co, Mn) Nanoparticles. *Journal of the American Chemical Society* **2004**, 126, 273-279
49. Evans, C. W.; Fitzgerald, M.; Clemons, T. D.; House, M. J.; Padman, B. S.; Shaw, J. A.; Saunders, M.; Harvey, A. R.; Zdyrko, B.; Luzinov, I.*, et al.* Multimodal Analysis of Pei-Mediated Endocytosis of Nanoparticles in Neural Cells. *ACS Nano* **2011**, 5, 8640-8648
50. Ho, D.; Fitzgerald, M.; Bartlett, C. A.; Zdyrko, B.; Luzinov, I. A.; Dunlop, S. A.Swaminathan Iyer, K. The Effects of Concentration-Dependent Morphology of Self-Assembling Rada16 Nanoscaffolds on Mixed Retinal Cultures. *Nanoscale* **2011**, 3, 907-910
51. Szymanski, C. R.; Chiha, W.; Morellini, N.; Cummins, N.; Bartlett, C. A.; O'Hare Doig, R. L.; Savigni, D. L.; Payne, S. C.; Harvey, A. R.; Dunlop, S. A.*, et al.* Paranode Abnormalities and Oxidative Stress in Optic Nerve Vulnerable to Secondary Degeneration: Modulation by 670 Nm Light Treatment. *PLoS ONE* **2013**, 8, e66448
52. Phokeo, V.; Kwiecien, J. M.Ball, A. K. Characterization of the Optic Nerve and Retinal Ganglion Cell Layer in the Dysmyelinated Adult Long Evans Shaker Rat: Evidence for Axonal Sprouting. *The Journal of Comparative Neurology* **2002**, 451, 213-224
53. Fitzgerald, M.; Bartlett, C. A.; Payne, S. C.; Hart, N. S.; Rodger, J.; Harvey, A. R.Dunlop, S. A. Near Infrared Light Reduces Oxidative Stress and Preserves Function in Cns Tissue Vulnerable to Secondary Degeneration Following Partial Transection of the Optic Nerve. *Journal of Neurotrauma* **2010**, 27, 2107-2119
54. Clode, P. L.Marshall, A. T. Variation in Skeletal Microstructure of the Coral Galaxea Fascicularis: Effects of an Aquarium Environment and Preparatory Techniques. *The Biological Bulletin* **2003**, 204, 138-145
55. Lechene, C.; Hillion, F.; McMahon, G.; Benson, D.; Kleinfeld, A.; Kampf, J. P.; Distel, D.; Luyten, Y.; Bonventre, J.; Hentschel, D.*, et al.* High-Resolution Quantitative Imaging of Mammalian and Bacterial Cells Using Stable Isotope Mass Spectrometry. *Journal of Biology* **2006**, 5, 20
56. Tsyalkovsky, V.; Klep, V.; Ramaratnam, K.; Lupitskyy, R.; Minko, S.Luzinov, I. Fluorescent Reactive Core–Shell Composite Nanoparticles with a High Surface Concentration of Epoxy Functionalities. *Chemistry of Materials* **2007**, 20, 317-325
57. Reukov, V.; Maximov, V.Vertegel, A. Proteins Conjugated to Poly(Butyl Cyanoacrylate) Nanoparticles as Potential Neuroprotective Agents. *Biotechnology and Bioengineering* **2011**, 108, 243-252
58. Lozić, I., Hartz, R.V., Bartlett, C.A., Shaw, J.A., Archer, M., Smith. N.M., Dunlop, S.A., Iyer, K.S., Kilburn. M.R. and Fitzgerald, M. Characterisation of Polymeric Nanoparticles for Treatment of Partial Injury to the Central Nervous System. *Data in Brief* **submitted**,
59. Salvati, A.; Pitek, A. S.; Monopoli, M. P.; Prapainop, K.; Bombelli, F. B.; Hristov, D. R.; Kelly, P. M.; Aberg, C.; Mahon, E.Dawson, K. A. Transferrin-Functionalized Nanoparticles

Lose Their Targeting Capabilities When a Biomolecule Corona Adsorbs on the Surface. *Nature Nanotechnology* **2013**, 8, 137-143
60. Hühn, D.; Kantner, K.; Geidel, C.; Brandholt, S.; De Cock, I.; Soenen, S. J. H.; Rivera-Gil, P.; Montenegro, J.-M.; Braeckmans, K.; Müllen, K.*, et al.* Polymer-Coated Nanoparticles Interacting with Proteins and Cells: Focusing on the Sign of the Net Charge. *ACS Nano* **2013**, 7, 3253-3263
61. Rutili, G.Arfors, K.-E. Protein Concentration in Interstitial and Lymphatic Fluids from the Subcutaneous Tissue. *Acta Physiologica Scandinavica* **1977**, 99, 1-8
62. Saptarshi, S.; Duschl, A.Lopata, A. Interaction of Nanoparticles with Proteins: Relation to Bio-Reactivity of the Nanoparticle. *Journal of Nanobiotechnology* **2013**, 11, 26
63. Jannin, B.; Menzel, M.; Berlot, J.-P.; Delmas, D.; Lançon, A.Latruffe, N. Transport of Resveratrol, a Cancer Chemopreventive Agent, to Cellular Targets: Plasmatic Protein Binding and Cell Uptake. *Biochemical Pharmacology* **2004**, 68, 1113-1118
64. N'soukpoé-Kossi, C. N.; St-Louis, C.; Beauregard, M.; Subirade, M.; Carpentier, R.; Hotchandani, S.Tajmir-Riahi, H. A. Resveratrol Binding to Human Serum Albumin. *Journal of Biomolecular Structure and Dynamics* **2006**, 24, 277-283
65. Cao, S.; Wang, D.; Tan, X.Chen, J. Interaction between Trans-Resveratrol and Serum Albumin in Aqueous Solution. *Journal of Solution Chemistry* **2009**, 38, 1193-1202
66. Liu, X.; Shang, Y.; Ren, X.Li, H. Molecular Modeling and Spectroscopic Studies on the Interaction of Transresveratrol with Bovine Serum Albumin. *Journal of Chemistry* **2013**, 2013, 7
67. Clode, P. L.; Stern, R. A.Marshall, A. T. Subcellular Imaging of Isotopically Labeled Carbon Compounds in a Biological Sample by Ion Microprobe (Nanosims). *Microscopy Research and Technique* **2007**, 70, 220-229
68. Song, C. X.; Labhasetwar, V.; Murphy, H.; Qu, X.; Humphrey, W. R.; Shebuski, R. J.Levy, R. J. Formulation and Characterization of Biodegradable Nanoparticles for Intravascular Local Drug Delivery. *Journal of Controlled Release* **1997**, 43, 197-212
69. Lee, H. J.Bae, Y. Pharmaceutical Differences between Block Copolymer Self-Assembled and Cross-Linked Nanoassemblies as Carriers for Tunable Drug Release. *Pharmaceutical Research* **2013**, 30, 478-488
70. Mori, S.Leblond, C. P. Electron Microscopic Features and Proliferation of Astrocytes in the Corpus Callosum of the Rat. *The Journal of Comparative Neurology* **1969**, 137, 197-225
71. Halonen, S. K.; Weiss, L. M.Chiu, F.-C. Association of Host Cell Intermediate Filaments with Toxoplasma Gondii Cysts in Murine Astrocytes in Vitro. *International Journal for Parasitology* **1998**, 28, 815-823
72. Robinson, J. M.; Karnovsky, M. L.Karnovsky, M. J. Glycogen Accumulation in Polymorphonuclear Leukocytes, and Other Intracellular Alterations That Occur During Inflammation. *The Journal of Cell Biology* **1982**, 95, 933-942
73. Ruge, C. A.; Kirch, J.; Cañadas, O.; Schneider, M.; Perez-Gil, J.; Schaefer, U. F.; Casals, C.Lehr, C.-M. Uptake of Nanoparticles by Alveolar Macrophages Is Triggered by Surfactant Protein A. *Nanomedicine: Nanotechnology, Biology and Medicine* **2011**, 7, 690-693
74. Lesniak, A.; Campbell, A.; Monopoli, M. P.; Lynch, I.; Salvati, A.Dawson, K. A. Serum Heat Inactivation Affects Protein Corona Composition and Nanoparticle Uptake. *Biomaterials* **2010**, 31, 9511-9518
75. Larson, T. A.; Joshi, P. P.Sokolov, K. Preventing Protein Adsorption and Macrophage Uptake of Gold Nanoparticles Via a Hydrophobic Shield. *ACS Nano* **2012**, 6, 9182-9190

76. Shang, L.; Nienhaus, K.Nienhaus, G. Engineered Nanoparticles Interacting with Cells: Size Matters. *Journal of Nanobiotechnology* **2014**, 12, 5
77. Turk, M. J.; Waters, D. J.Low, P. S. Folate-Conjugated Liposomes Preferentially Target Macrophages Associated with Ovarian Carcinoma. *Cancer Letters* **2004**, 213, 165-172
78. Lunov, O.; Syrovets, T.; Loos, C.; Beil, J.; Delacher, M.; Tron, K.; Nienhaus, G. U.; Musyanovych, A.; Mailänder, V.; Landfester, K.*, et al.* Differential Uptake of Functionalized Polystyrene Nanoparticles by Human Macrophages and a Monocytic Cell Line. *ACS Nano* **2011**, 5, 1657-1669
79. Yan, Y.; Gause, K. T.; Kamphuis, M. M. J.; Ang, C.-S.; O'Brien-Simpson, N. M.; Lenzo, J. C.; Reynolds, E. C.; Nice, E. C.Caruso, F. Differential Roles of the Protein Corona in the Cellular Uptake of Nanoporous Polymer Particles by Monocyte and Macrophage Cell Lines. *ACS Nano* **2013**, 7, 10960-10970
80. Perekatt, A. O.; Valdez, M. J.; Davila, M.; Hoffman, A.; Bonder, E. M.; Gao, N.Verzi, M. P. Yy1 Is Indispensable for Lgr5+ Intestinal Stem Cell Renewal. *Proceedings of the National Academy of Sciences* **2014**, 111, 7695-7700
81. Fitzgerald, M.; Payne, S. C.; Bartlett, C. A.; Evill, L.; Harvey, A. R.Dunlop, S. A. Secondary Retinal Ganglion Cell Death and the Neuroprotective Effects of the Calcium Channel Blocker Lomerizine. *Invest Ophthalmol Vis Sci* **2009**, 50, 5456-62
82. Savigni, D. L.; O'Hare Doig, R. L.; Szymanski, C. R.; Bartlett, C. A.; Lozic, I.; Smith, N. M.Fitzgerald, M. Three Ca Channel Inhibitors in Combination Limit Chronic Secondary Degeneration Following Neurotrauma. *Neuropharmacology* **2013**, 75C, 380-390

Figure 1

Click here to download Figure: P2_Fig1 final.eps

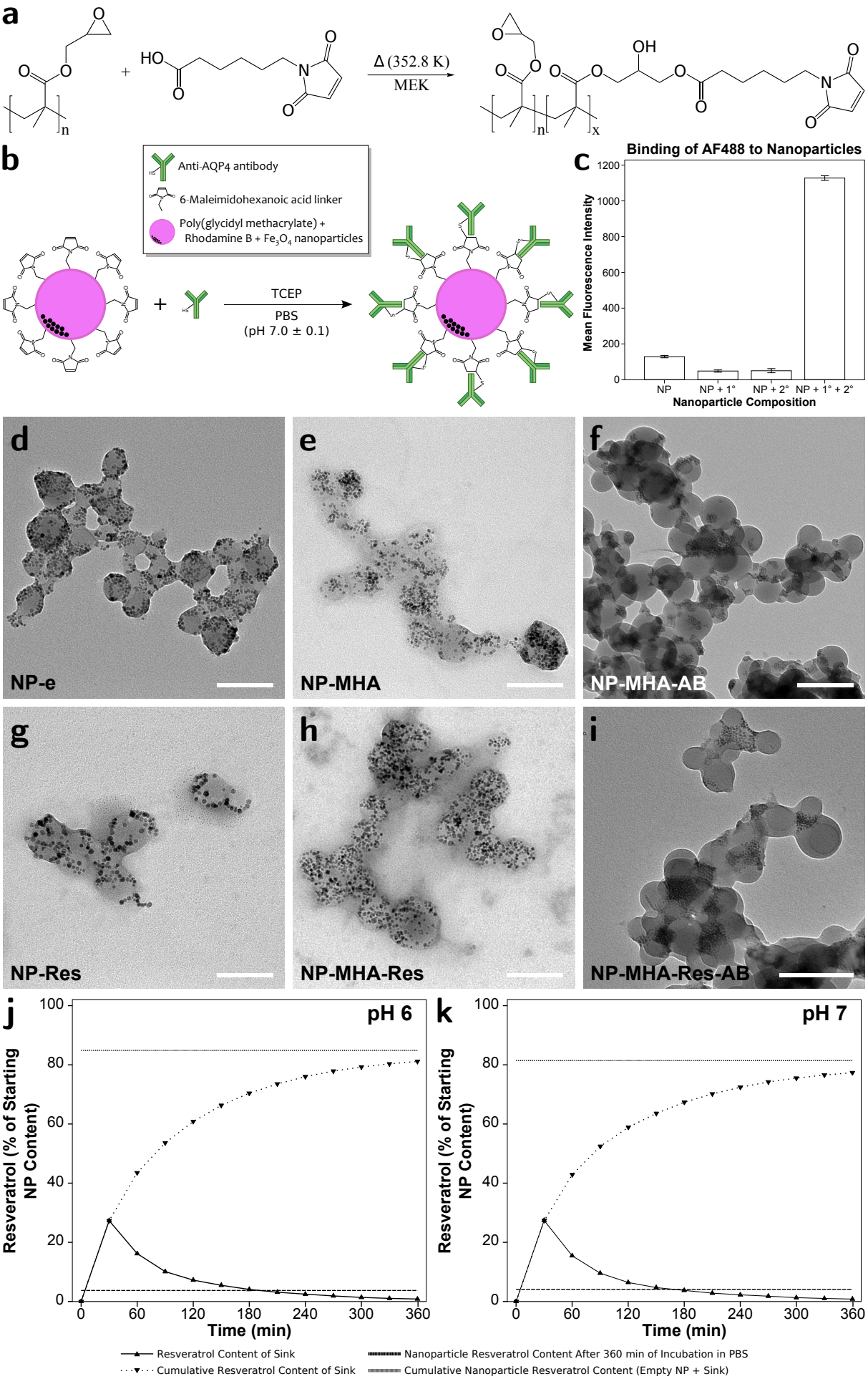

Figure 2

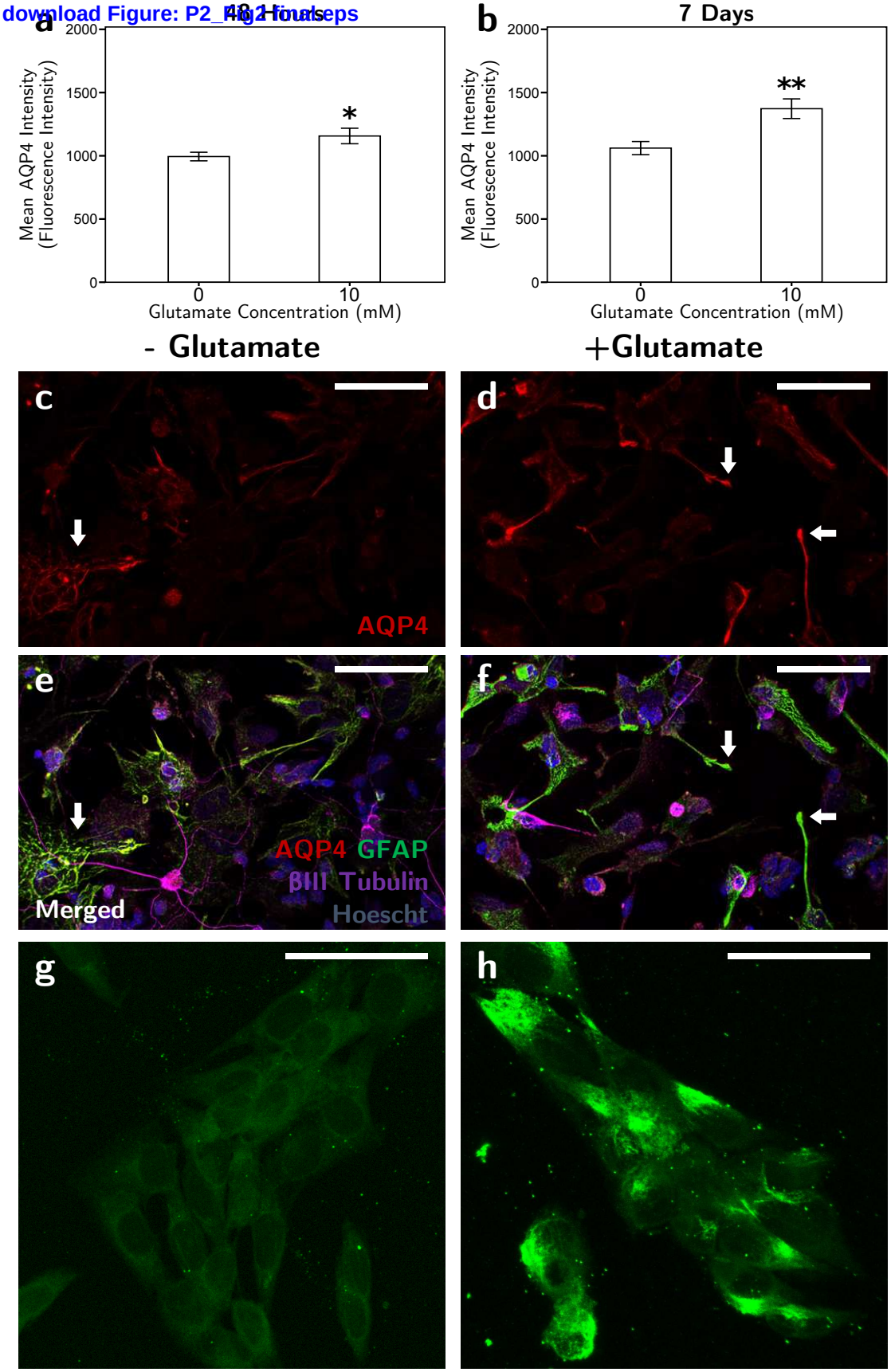

Figure 3

Click here to download Figure: P2_Fig3 final.eps

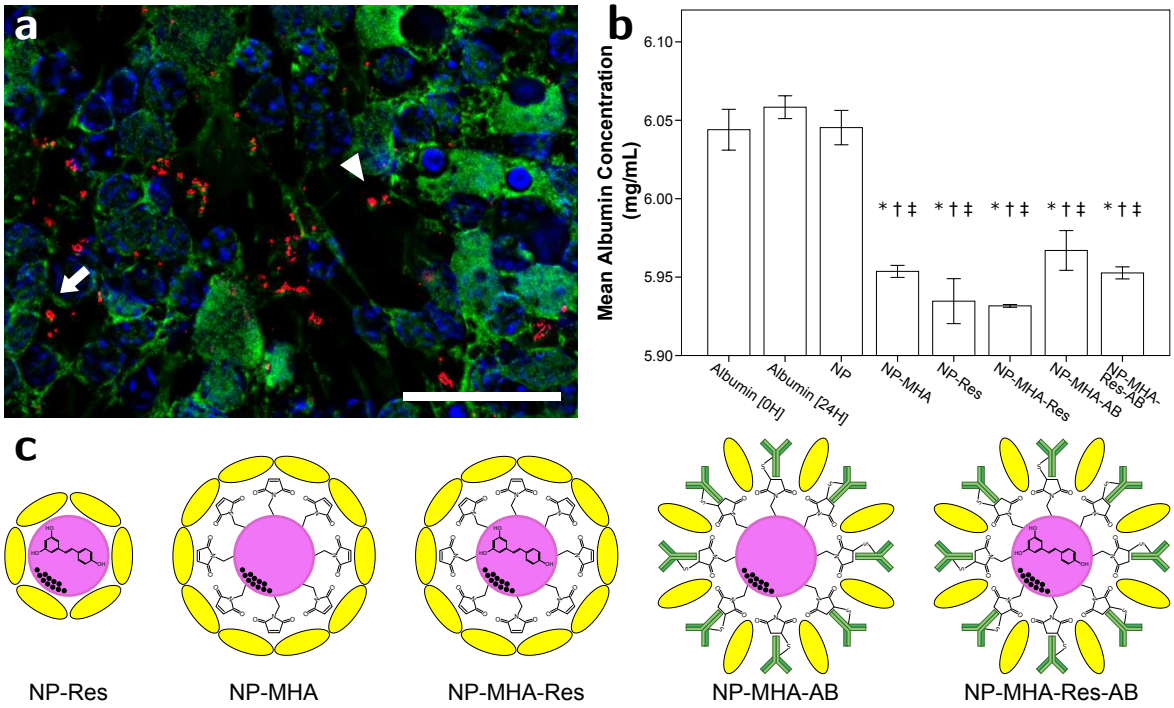

Figure 4
Click here to download Figure: P2_Fig4 final.eps

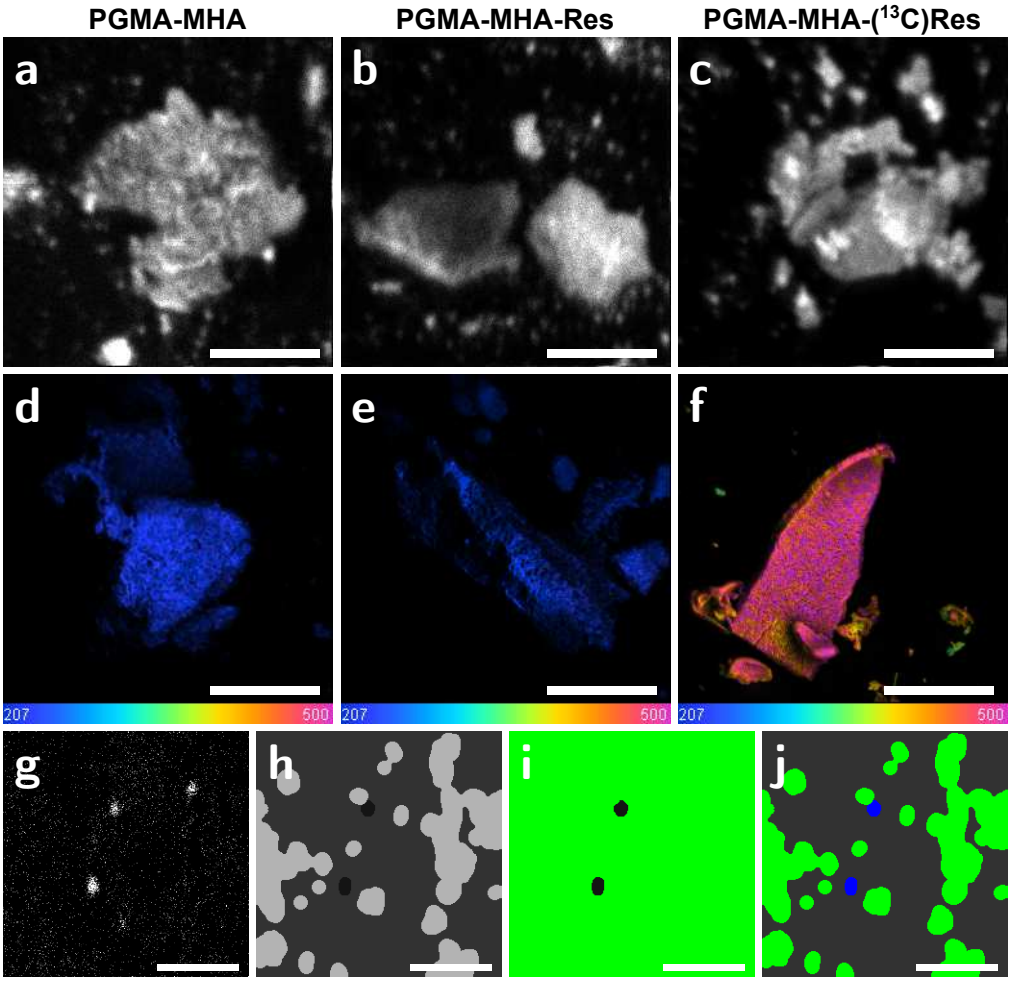

Figure 3

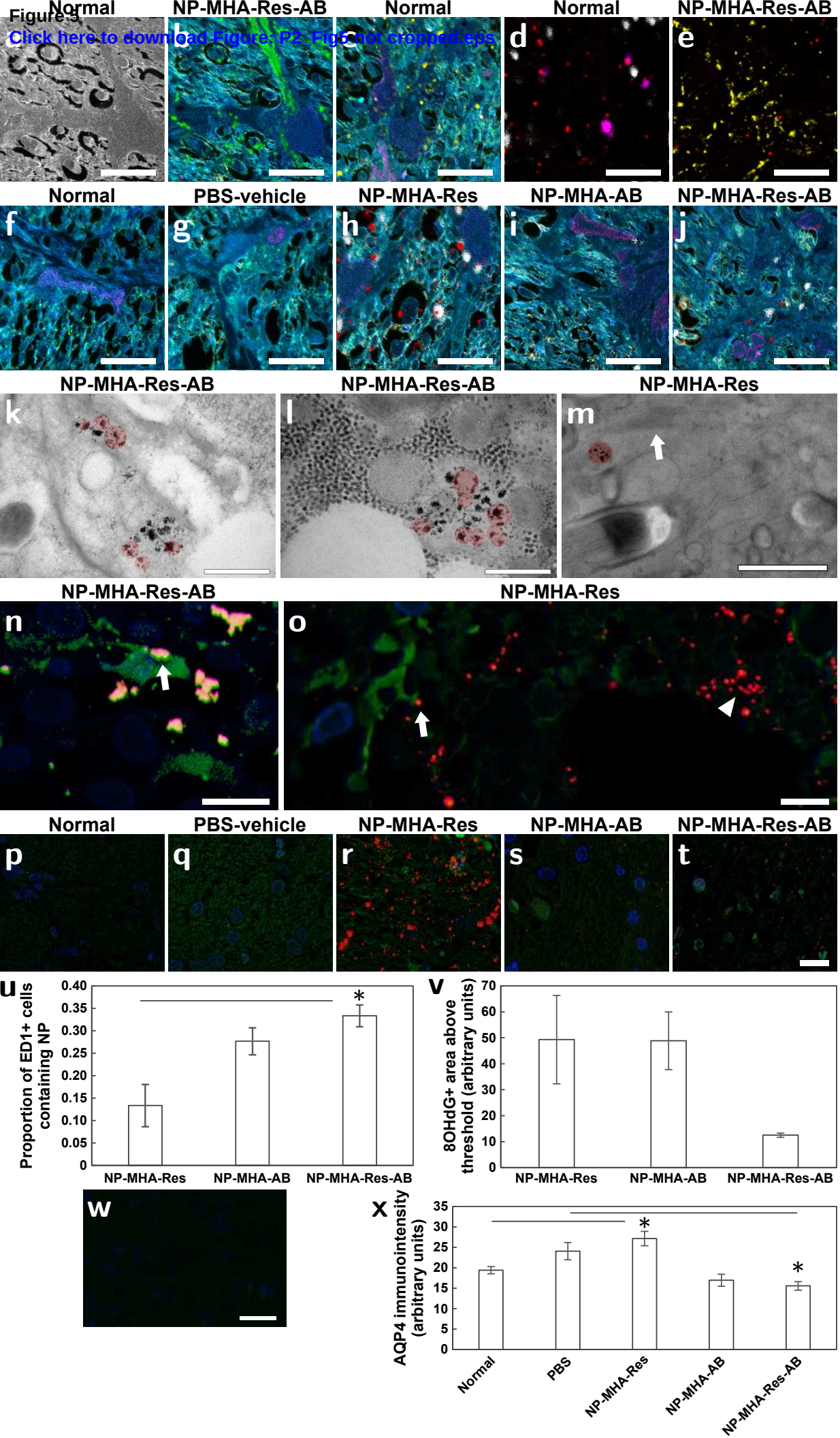

Figure 6

Click here to download Figure: P2_Fig6 final.eps

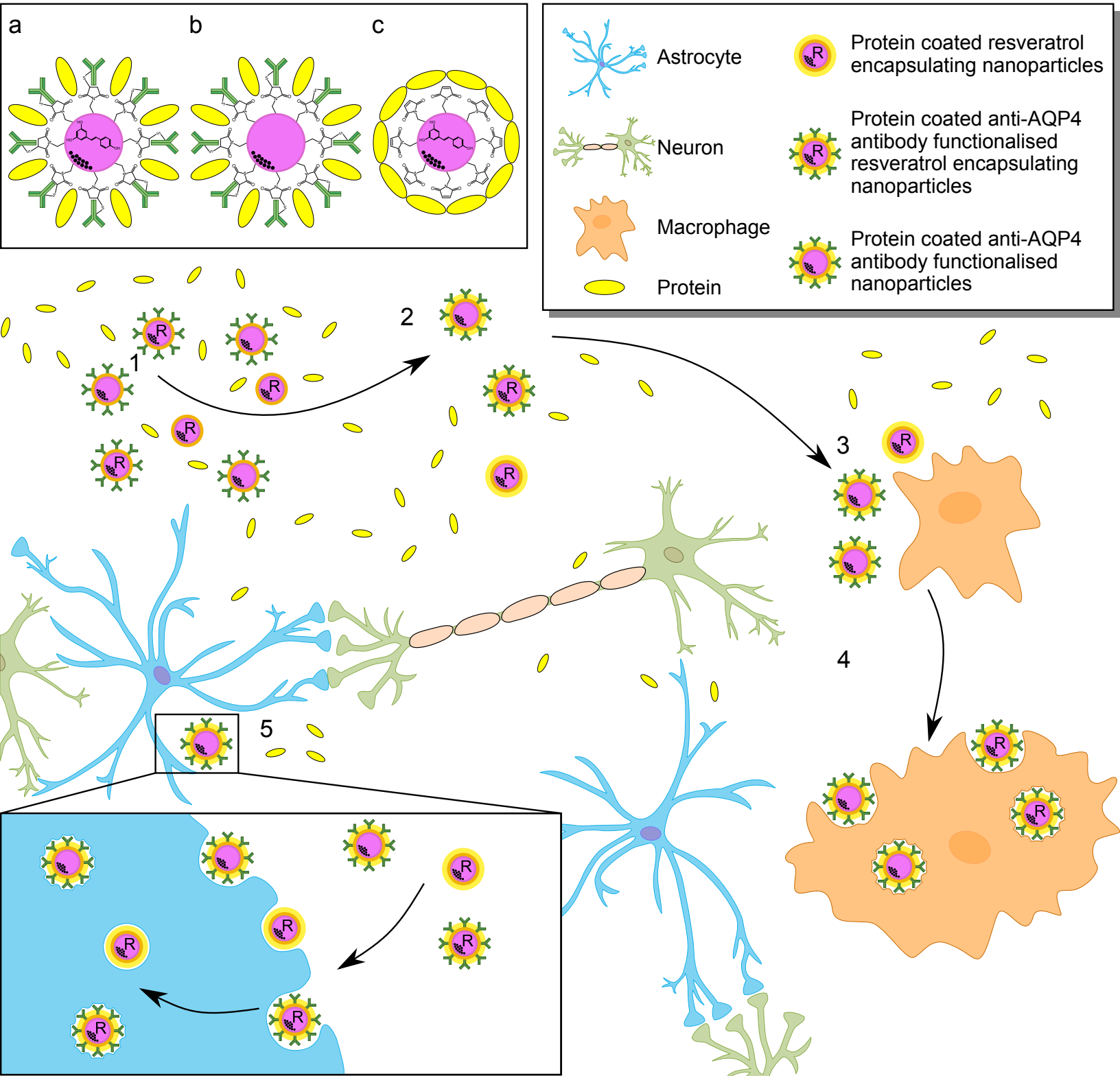

Figure 7
Click here to download Figure: P2_Fig7 final.eps